Cretaceous climate change evidenced in the Senegalese rock record, NW Africa

Pearson, M.; Casson, M.; Millar, I.; Charton, R.; Redfern, J.

DOI
10.1016/j.jafrearsci.2023.105166

Publication date
2024

Document Version
Final published version

Published in
Journal of African Earth Sciences

Journal of African Earth Sciences 211 (2024) 105166

Contents lists available at ScienceDirect

Journal of African Earth Sciences

journal homepage: www.elsevier.com/locate/jafrearsci

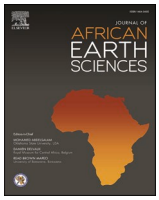

Cretaceous climate change evidenced in the Senegalese rock record, NW Africa

M. Pearson [a,b,*,1], M. Casson [a,c], I. Millar [d], R. Charton [a,e], J. Redfern [a]

[a] North Africa Research Group (NARG), Department of Earth and Environmental Sciences, The University of Manchester, Williamson Building, Oxford Road, Manchester, M13 9PL, UK
[b] Mineralogy Facility, British Geological Survey, Keyworth, Nottingham, NG12 5GG, UK
[c] Equinor ASA, Forus Vest, Svanholmen 8, 4313, Sandnes, Norway
[d] National Isotope Geoscience Laboratory, Kingsley Dunham Centre, Keyworth, Nottingham, NG12 5GG, UK
[e] Delft University of Technology (TU Delft), Mekelweg 5, 2628 CD, Delft, Netherlands

ARTICLE INFO

Handling Editor: Dr Mohamed Mohamed G Abdelsalam

Keywords:
Climate
Senegal
NW-Africa
Cretaceous
Ocean-anoxia
Clay-minerals

ABSTRACT

Climate change directly impacts the source, mode and volume of sediment generation which can be observed in the rock record. To accurately model source to sink systems, in addition to hinterland geology, tectonics and transport distance, a thorough comprehension of the climate is essential. In this study we evaluate the role of climate on Cretaceous sediment delivery into the Senegal Basin, NW Africa, using data recorded from extensive sampling of basinal sediments. This is achieved through the mineralogical characterisation by X-ray diffraction and $^{146}Nd/^{144}Nd$ and $^{86}Sr/^{88}Sr$ isotopic analyses, which are correlated against existing, climate, tectonic and oceanographic models.

Examples of climatic indicators include the change from predominantly smectitic deep marine basinal-clays recorded from the Cretaceous in DSDP wells 367 and 368 to clays with increased illite and kaolinite content, observed during the Albian and Cenomanian-Turonian, interpreted to be representative of higher humidity following the kaolinisation of hinterland source-rocks. Another climate indicator is the observation of palygorskite in deep-marine sediments, noted to be indicative of ocean anoxia related to the authigenesis of marine-smectite, a product of warm saline bottom waters and increased abundancy of silicon. The increase in salinity is interpreted to be a biproduct of elevated temperatures throughout the Cenomanian and increased denudation of the North Atlantic circumjacent continental evaporite-belts. Increase in silicon (biogenic) is related to a result of ocean-wide mass extinction of foraminifera during OAE2 triggered by the eruption of the Caribbean large igneous province.

The results suggest that Cretaceous climate evolution of Senegal can be divided into four stages: 1. Berriasian-Barremian; an arid-period with monsoonal weather producing modest fluvial systems restricted to coastal regions. 2. Aptian-Albian; the establishment of a paleo-Intertropical Convergence Zone began to increase global temperature and humidity as recognised by the increase in kaolinite content. 3. Cenomanian-Turonian; the Cretaceous Thermal Maximum hothouse period incurring exceptional temperatures and humidity. This is represented as an antithetical shift in clay mineralogy from chlorite-illite to smectite-kaolinite throughout most of the onshore and nearshore basinal sediments. 4. Coniacian-Maastrichtian; transitional from tropical-to-tropical swamp-like conditions evidenced by increased onshore basin sediment capture and a shift in vegetation to aquatic-fern species.

The impact of climate change throughout the Cretaceous produced dynamic shifts in both river size and source-catchment, witnessing exception rates of denudation during the hotter and more humid periods, which climaxed during the Cenomanian and Turonian as a result of the Cretaceous Thermal Maximum. This eroded sediment was deposited in both the onshore and offshore basins during the mid-late Cretaceous but became increasingly restricted to the onshore segment of the basin during the Late Cretaceous.

* Corresponding author. North Africa Research Group (NARG), Department of Earth and Environmental Sciences, The University of Manchester, Williamson Building, Oxford Road, Manchester, M13 9PL, UK.
E-mail address: iaian1@bgs.ac.uk (M. Pearson).
[1] (formally, Mounteney, I).

https://doi.org/10.1016/j.jafrearsci.2023.105166
Received 16 June 2023; Received in revised form 19 December 2023; Accepted 19 December 2023
Available online 25 December 2023

1. Introduction

Climate change, a dynamic process throughout Earth's history, is influenced by several factors including tectonism (e.g., Müller and Dutkiewicz, 2018; Hay and Floegal, 2012), volcanism (e.g., Buchs et al., 2018; Robock and Outten,), atmospheric changes (e.g., Holz et al., 2015) and fluctuations in planetary eccentricity, obliquity and precession (e.g., Park et al., 1993; Liu et al., 2020). Changes in climate has a profound effect on the mode of hinterland denudation and the volume and transportation mechanisms for the exhumed sediment (Farrant et al., 2019). Tectonics also contributes towards hinterland denudation with regional uplift. Dynamic topography at a plate scale undoubtably also has an influence on climate, through changes in oceanography, volcanism and meteorology.

During the Phanerozoic, there have been five major "hothouse" periods: in the Cambro-Ordovician (Landing, 2012), the Middle Devonian (Tuite et al., 2019), the Triassic (Winguth et al., 2015), the Cretaceous Cenomanian-Turonian transition, known as the Cretaceous Thermal Maximum (CTM; Haq and Huber, 2017), and the Palaeocene-Eocene Thermal Maximum (PETM; Kemp et al., 2016). The Cretaceous was a dynamic period of global climate change, where the Earth experienced a gradual increase in global average temperatures, from a warm *ca.*20 °C during the Berriasian to a ~24 °C "hothouse" (Scotese, 2021; Martin et al., 2014) during the Cenomanian-Turonian, which translated to tropical sea-surface temperatures of >33 °C (Poulsen et al., 2013) and potentially as high as 42 °C in the equatorial region of the Demerara Rise (Hay & Floegal et al., 2012). The CTM average global temperature began to decline during the Santonian (Late Cretaceous) and the Earth's climate changed dramatically at the end of the Cretaceous at the K/T boundary event, interpreted to be a result of the Chicxulub meteor impact (Whalen et al., 2020), Nadir impact offshore West Africa (Nicholson et al., 2022) and the near-simultaneous eruption of the Deccan-Trap Large Igneous Province (LIP; Chiarenza et al., 2020).

This study focuses on the Cretaceous equatorial climate established around the NW African conjugate margin; recorded in the sedimentary sequences within the Senegal/Gambia segment of the Mauritania-Senegal-Guinea-Bissau-Guinea-Conakry Basin (MSGBC Basin; Ndiaye et al., 2016; Casson et al., 2020a,b Mounteney et al., 2021, Fig. 1 C). The purpose of this study is to assess the impact climate change had on the sedimentary rock-record and to correlate, and define these changes through time. To achieve this aim both quantitative mineralogy of samples from DSDP and nearshore exploration-wells (Fig. 1 A, B) were analysed, together with corresponding εNd (0) and $^{87}Sr/^{86}Sr$ isotopes, to define sediment source and changes in climate throughout the Cretaceous.

The DSDP sites used in this study are 367 (Cape Verde Basin; Lamont-Doherty & Bukry, 1978a) and 368 (Cape Verde Rise; Lamont--Doherty & Bukry, 1978b) off the west coast of Senegal, Africa and 534 (Blake-Bahama Basin; Sheridan and Gradstein, 1980) off the east coast of Florida, North America. DSDP sites were chosen that sampled the post-rift Mesozoic stratigraphic sequences in the deep Atlantic Ocean Basin to allow correlation of climatic signatures between the eastern margin (DSDP 367 & 368) and the western margin (DSDP 534) of the oceanic basin. In addition, hydrocarbon exploration wells located adjacent to the modern-day coastlines of Senegal and The Gambia are used to constrain sedimentation from the MSGBC Basin deep (neritic) facies in the Cretaceous, that were also examined to identify shifts in climatic trends (Table 1).

As exemplified by a recent body of studies from Morocco to Mauritania (north of the study area), the Cretaceous is a period of voluminous delivery of eroded clastic material into the Atlantic coastal basins (e.g., Luber et al., 2018; Arantegui et al., 2019), of substantial

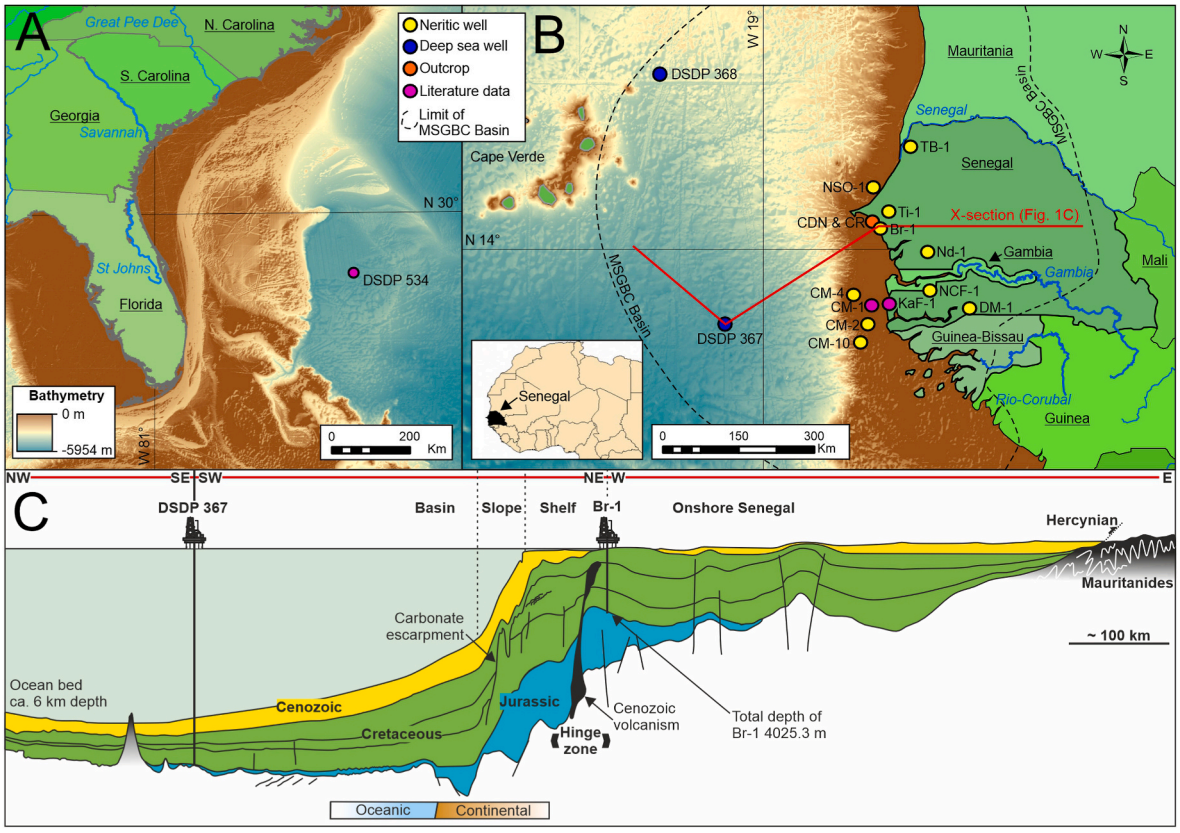

Fig. 1. Study well locations: A, DSDP 534 (Blake Bahama Ridge). B, location of DSDP 367 (Cape Verde Basin) & 368 (Cap Verde Rise), nearshore wells and coastal exposures of the west coast of Senegal, NW Africa. C, Schematic cross section through NW African Atlantic passive margin, highlighting the main stratigraphic packages and architecture of the MSGBC Basin (Modified from Casson et al., 2020a).

shifts in sedimentary source domains (e.g., Charton et al., 2021), associated with higher than predicted exhumation in the passive margin hinterlands (e.g., Gouiza et al., 2019; Charton et al., 2018). A combination of atmospheric (landmass distribution and palaeolatitudes plate drift), surface (erodibility variation), lithospheric (onset of the South Atlantic oceanic drift) and asthenospheric (dynamic topography) processes has been proposed to account for the superimposed wavelength of vertical movement patterns (Charton, 2018).

2. Review

2.1. Oceanography

Several key oceanographic events occurred throughout the Jurassic and Cretaceous, the most important of these being the establishment of the Equatorial Atlantic Gateway (EAG) linking the Northern and Southern Atlantic Oceans (Pletsch et al., 2001). During this period of growth of the Atlantic seafloor through Mid Ocean Ridge Basalt (MORB) volcanism (Fig. 2), several Oceanic Anoxic Events (OAE) occurred (Fig. 2). These periods of ocean anoxia are believed to have occurred as a consequence of reduced oceanic-circulation, climate warming and associated increases in greenhouse gases; all of which have profound links to Large Igneous Province (LIP) volcanism. These OAE's vary in scale and longevity, with well documented regional to global scale depletion of dissolved oxygen within the oceans, leading to anoxic/euxinic submarine environments (Danzelle et al., 2018). Anoxic events correspond with periods of mass extinction and/or the deposition of black shales across the Earth (Hülse et al., 2019; Gertsch et al., 2010; Dodsworth et al., 2020; Fathy et al., 2023).

Three global anoxic events occurred during the Cretaceous: the Weissert OAE during the Valanginian (Bottini et al., 2018), OAE1a in the Aptian (121 Ma, Adloff et al., 2020) and OAE2 which occurred during the Cenomanian-Turonian transition, coinciding with peak temperatures during the CTM. The Weissert OAE was also a short-lived event, occurring between 132.7 and 133.8Ma (Bottini et al., 2018) and is believed to have resulted from the Piranha LIP in South America. OAE1a occurred ~121Ma and lasted for 0.5–1.0Ma (Leckie et al., 2002) and is associated with the Ontong Java LIP in the southwestern Pacific Ocean (Taylor, 2006). OAE2 occurred during the Cenomanian-Turonian transition (90-84 Ma) and whilst a direct magmatic proxy preserved in the sedimentary record has yet to be found, osmium isotopes (Pogge von Strandmann et al., 2013) clearly demonstrate that a widespread magmatic event (Caribbean LIP; Buchs et al., 2018 and High Artic LIP (Lobkovsky et al., 2013) occurred prior to the onset of OAE2 (Turgeon and Creaser, 2008). Smaller regional-scale anoxic events include OAE1b (~111 Ma), OAE1d (~100 Ma) and OAE3 (~86 Ma) (Huber et al., 2018; Wagreich, 2012).

Early in the Cretaceous, North and South America Continental masses may have been separated sufficiently to allow an Atlantic-Pacific westward marine current to form (Hay, 2009; Sewall et al., 2007). This westward current is suggested to have diminished in the Cenomanian with the emplacement of the Caribbean LIP (Buchs et al., 2018). The combination of restricted circulation, increased evapotranspiration, (related to rising global temperatures) and increased ocean salinity, reversing the thermohaline circulation producing large volumes of dense Warm Saline Bottom Waters (WSBW; Hay and Floegal, 2012) and anoxic/euxinic conditions. North Atlantic Ocean salinity was raised further by increased denudation of the North Atlantic circumjacent continental evaporite-belts (Hay and Floegal, 2012). High levels of marine productivity are interpreted to be due to increased nutrients sourced from continental weathering as a consequence of elevated temperature and humidity, that provided additional organic matter in the north Atlantic Basin. This increase in organic matter, which was respired at the expense of oxygen (and other oxidants), exacerbated oceanic anoxia (Monteiro et al., 2012). These changes of oceanic conditions combined with outgassing of volcanic CO_2 would have been the main drivers for the OAE2.

Cretaceous sea-levels were 50–100m higher during the very-Early Cretaceous compared to modern-day, ~150m higher during the Aptian and Albian, and up to ~200m higher during the Late Cretaceous (Fig. 2). This eustatic rise in sea-level has been attributed to melting of polar ice, volume changes in oceanic basins due to LIP emplacement, increased sedimentation, basement uplift and increases in ocean ridge volume (Wright et al., 2020). The maximum sea-level increase (~200 m) occurred throughout the CTM and again in the late Campanian. During these periods, vast epicontinental seas such as the Western Interior Seaway of North America (Lowery et al., 2018) and trans-Saharan Seaway of North Africa (Morsi et al., 2008) were formed. However, whilst large epicontinental seaways existed throughout much of the globe during the Late Cretaceous, marine transgression failed to encroach significantly eastwards into the onshore segment of the Senegalese Basin, as evidenced by large submarine fan systems throughout the Aptian and Turonian, primarily adjacent to the exit of the modern-day Senegal River to the north of Senegal (Fig. 11 B, C, D), several smaller sediment bypass-channel lobes during the Campanian (Fig. 11 E) and smaller coastal fan-deposits during the Maastrichtian (Fig. 11 F). These well-defined fans (Casson et al., 2020c) could not have formed if marine transgression had flooded the onshore basin. There is also no significant change in sedimentary facies throughout the onshore-basin (Fig. 4) which may be characteristic of marine transgression.

Table 1
Sample locations.

Location name	Location ID	Region	Location type	Latitude	Longitude	Data acquisition
DSDP534	DSDP534	Blake-Bahama Ridge	Well	28°20.6″N	75°22.9″W	Chamley et al. (1983)
DSDP367	DSDP367	Cape Verde Basin	Well	12°29.2″N	20°02.8″W	This work & Mourlot et al., 2018b
DSDP368	DSDP368	Cape Verde Rise	Well	17°30.4″N	21°21.2″W	This work & Mourlot et al., 2018b
M'Bour-1	Br-1	MSGBC Basin	Well	14°25′0.75″N	16°58′1.11″W	This work
Casamance Maritime-1	CM-1	MSGBC Basin	Well	12°49′38.32″N	17°10′51.91″W	Mourlot et al., 2018b
Casamance Maritime-2	CM-2	MSGBC Basin	Well	12°30′9.07″N	17° 5′40.43″W	This work
Casamance Maritime-4	CM-4	MSGBC Basin	Well	12°45′27.10″N	17°24′43.14″W	This work
Casamance Maritime-10	CM-10	MSGBC Basin	Well	12°13′25.09″N	17°14′36.41″W	This work
Diana Malari-1	DM-1	MSGBC Basin	Well	12°49′42.42″N	15°11′16.31″W	This work
Kafountine-1	KaF-1	MSGBC Basin	Well	12°49′38.28″N	16°46′36.25″W	Chamley et al. (1988)
Nord Casamance F-1	NCF-1	MSGBC Basin	Well	13°10′18.57 N	15°59′58.53 W	This work
North Senegal Offshore-1	NSO-1	MSGBC Basin	Well	15°14′43.28″N	16°59′42.09″W	This work
Tienaba-1	Ti-1	MSGBC Basin	Well	14°47′17.88″N	16°42′35.76″W	This work
Toundou-Besset-1	TB-1	MSGBC Basin	Well	16°13′3.38″N	16°23′12.94″W	This work
Cap Rouge	CR	Senegal coast	Outcrop	14°38′6.46″N	17°10′24.33″W	This work
Cap de Naze	CDN	Senegal coast	Outcrop	14°32′19.36″N	17°6′15.28″W	This work

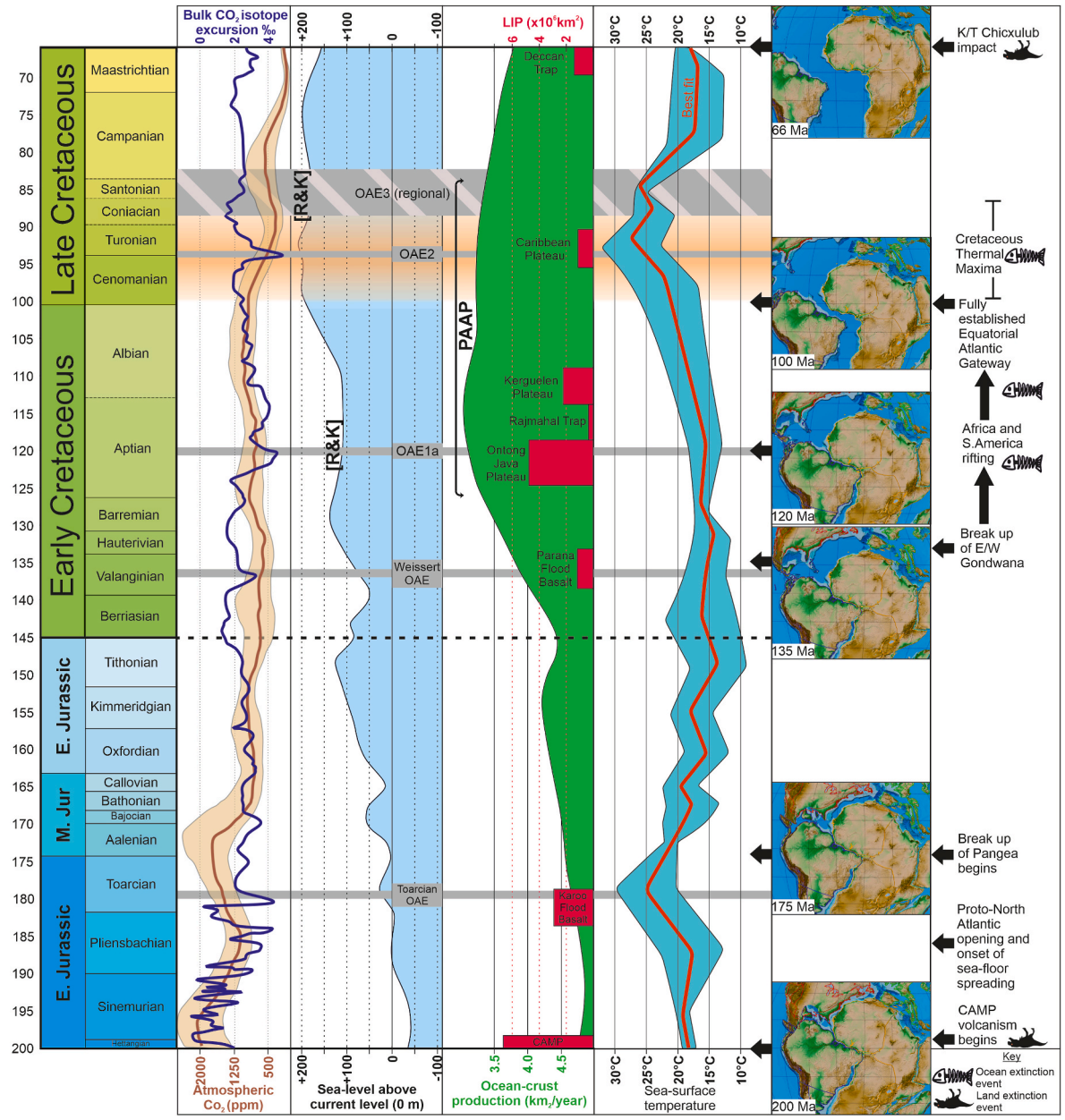

Fig. 2. Jurassic to Cretaceous geological and environmental log. Atmospheric CO_2 concentrations from Müller and Dutkiewicz (2018). Bulk CO_2 isotope excursion, sea-level and magmatism from Takashima et al. (2006). Sea surface temperatures from Martin et al. (2014). R&K (regression and associated karstification of Senegalese platform carbonates). PAAP = Peri-Atlantic Alkaline Pulse (Matton and Jébrak, 2009). Landmass positions created using G-Plates (ver 2.3).

2.2. Tectonism

Tectonism during the Early Jurassic (c. 200 Ma) is associated with a major episode of tholeiitic volcanism in the Central Atlantic Magmatic Province (CAMP; Marzoli et al., 1999) marking the beginning of the breakup of Pangea, which produced one of the Earth's largest ever continental LIPs (Svensen et al., 2017). CAMP magmatism triggered the opening of the proto-Central Atlantic Ocean approximately 185 Ma, with the onset of seafloor spreading (Labails et al., 2010; Torsvik et al., 2008).

A subsequent major stage of tectonism that occurred throughout the Cretaceous Period (Scotese, 2004; Rogers and Santosh, 2003) was associated with the separation of Eastern Gondwana (Antarctica, Australia and India) from Western Gondwana (Africa and South America). During the Valanginian (~133 Ma), "Atlantica" (the 2.2 Ga ancient continent described by Rogers (1996), which encompasses the Archean Guyana/Brazilian, São Francisco, and Rio de la Plata cratons of South America, and West African, West Nile and Congo cratons of Africa) entered into a diachronous rifting phase propagating from south to north (Pletsch et al., 2001; Labails et al., 2010; Torsvik et al., 2008) resulting in the opening of the proto-South Atlantic Ocean and the eventual formation of the Equatorial Atlantic Gateway. The EAG evolved from a shallow marine gateway during the Albian, to a fully established deep-water oceanic connection linking the northern and southern Atlantic Oceans during the Cenomanian (Pletsch et al., 2001).

The reason the Cretaceous marine transgression did not extend into the onshore Senegalese Basin is interpreted to be due to tectonic uplift. The possible tectonic processes can be divided into prerift and post-rift phases. During the pre-rift stage, upwelling of hot, buoyant asthenospheric magma can effectuate thermal expansion and associated crustal updoming (White and Mckenzie, 1989). However, typically, the study of passive-margin continental hinterland tectonics is mainly associated

with postrift processes, in which vertical displacements are indirectly linked to plate movements (Blenkinsop and Moore, 2013). Crustal underplating is another method which can affect dynamic topography, whereby the addition of rising basaltic magma with a density lower than the surrounding mantle increases the relative buoyancy of the continental margin (Blenkinsop and Moore, 2013). This crustal underplating can occur during conjugate margin rifting along the upper plate.

The Cretaceous (~125–80 Ma) was a dynamic period of increased tectonic activity that also coincides with the Cretaceous Peri Atlantic Alkaline Pulse (PAAP: Matton and Jébrak, 2009) and Western Central African Rift System (WCARS: Fairhead, 2023). All of these tectono-magmatic processes possess significant potential to induce dynamic topography along the conjugate margins. Surface and subsurface manifestations of this period of heightened tectono-magmatic activity is evidenced by the presence CAMP dykes and sills located extensively throughout both conjugate margins (Marzoli et al., 2018; Gilchrist and Summerfield, 1994, Fig. 11).

A dynamic uplift of >150–200m on the NW African conjugate margin would be sufficient to inhibit marine transgression during the Cretaceous. By comparison, crustal underplating and associated continental uplift is reported to have affected regions of the North Atlantic Tertiary Province (NATP) on either side of the present-day ocean, identified in Greenland, Norway, and Scotland. In the case of Scotland, Watson (1985) suggested the western part of the Scottish craton was uplifted during the Eocene by up to 1.5 km, an event associated with coeval North Atlantic volcanism (Cox, 1993). This suggests uplift of the order of >150–200m is plausible.

Additional evidence for the dynamic uplift of the NW African margin includes two periods of platform-shelf carbonate karstification, recognised during the Aptian and Senonian (Martin et al., 2010; Clayburn, 2018). The drop in relative sea-level occur during a period of rising sea levels, suggesting any coincident increases in dynamic topography was of a greater magnitude, leading to a period of marine regression and the subaerial exposure of the platform carbonates (Fig. 2). The increase in vertical displacement of the continental passive margin would be transient, with envisaged elevation-decay over a period of ~60Ma (Blenkinsop and Moore, 2013).

2.3. Meteorology

The modern-day thermal equator resides a few degrees north of the geographic equator, reflecting variation of landmass in the northern and southern hemispheres. The Intertropical Convergence Zone (ITCZ) represents a zone where warm air flows over the mid latitude convergence, gathering moisture from mid latitude oceans. The ITCZ broadly follows the periphery of the thermal equator with fluctuations northwards and southwards over time from the geographical equator due to seasonal and longer-term climatic variations related to the different thermal gradients between the underlying landmass and ocean basins. The amount of continental-rainfall is governed by the position of the seasonal ITCZ in relation to the humid Tropical Maritime Air-Masses and the dry Tropical Continental Air-Masses. As the humid Tropical Maritime Air-Masses rise, the moisture condenses into cumulonimbus clouds, these clouds rise further, producing orographic precipitation over the windward slopes of the continental margin.

Whilst the position of the continents differed in the Cretaceous compared to their modern-day locations, these meteorological principals would have still applied. Convergence of surface winds during the Valanginian to Hauterivian (133Ma; Fig. 3 A) were determined through observations of aeolian cross-bedding directions by Scherer et al. (2020). The palaeo-ITCZ is predicted to shift profoundly, to ~S25° in the Central Atlantic, with the convergence of the humid Tropical Maritime

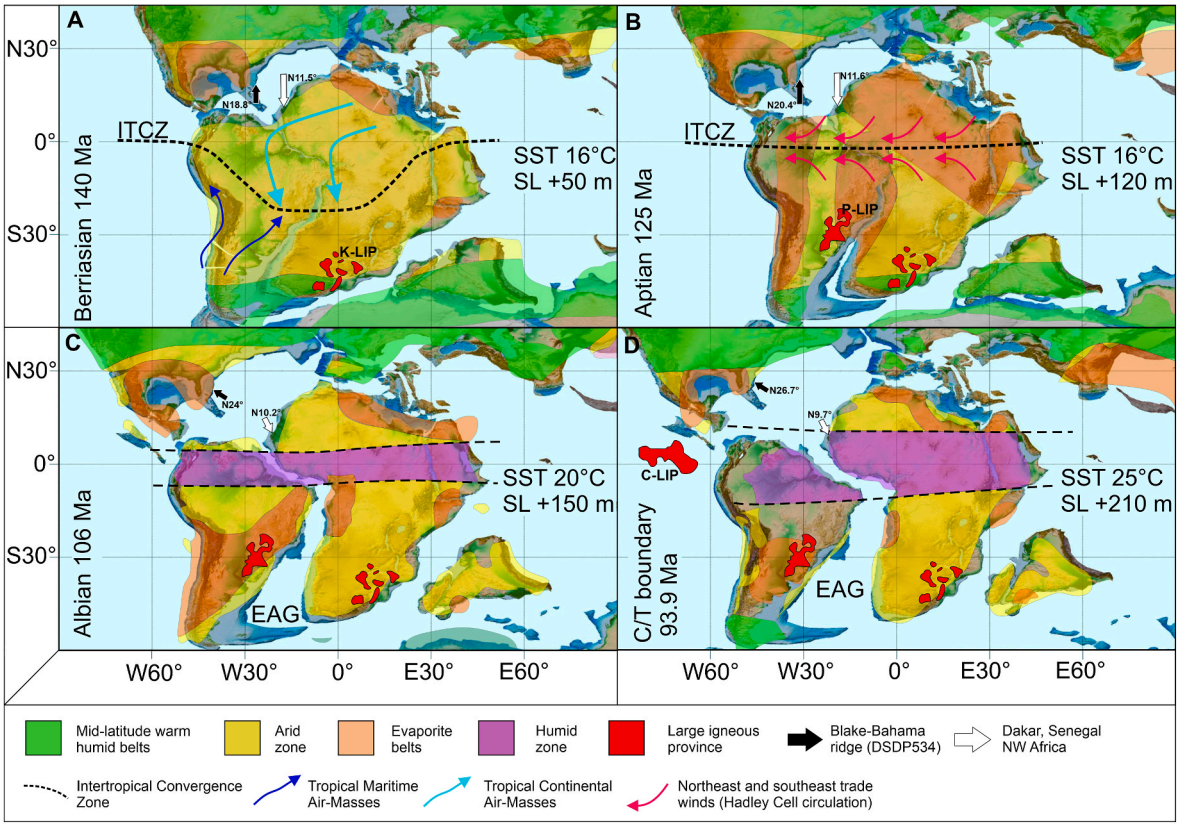

Fig. 3. Palaeo ITCZ establishment from the formation of Hadley cells during the Valanginian-Barremian (Scherer et al., 2020) and corresponding Cretaceous climate modelling modified by Hay and Floegal et al. (2012). K-LIP = Karoo LIP, P-LIP = Piranha LIP, C-LIP = Caribbean LIP, ITCZ (Intertropical convergence zone), EAG (Equatorial Atlantic Gateway), SST (Sea Surface Temperature) and SL (Sea-level).

Air-Masses from Panthalassa (Proto-Pacific Ocean) and the north-easterly Tropical Continental Air-Masses of northern-Africa. Most rainfall during this period would have been concentrated along the western margin of South America. Central Gondwana would have experienced limited rainfall, that led to vast areas of hot arid land, which has been described as the "supercontinent effect" (Hay and Floegal, 2012; and others within).

A consequence of these elevated temperatures may have also resulted in a "dead zone effect" whereby the climate is so warm that plant-life cannot perform photosynthesis regardless to the existence of available moisture (Hay and Floegal, 2012). Onshore precipitation was monsoonal with mean seasonal precipitation of 0–0.5 mm/day for Dec–Feb and 2–8 mm/day Jun–Aug (Sellwood and Valdes, 2006). Between the Valanginian and the Barremian the position of the palaeo-ITCZ gradually shifted from an Atlantica-concentric ITCZ to a zonal-equatorial circulation influenced by Hadley cell circulation (Fig. 3 B), evidenced by NW aeolian palaeo-currents in low latitude Gondwana (Scherer et al., 2020). The shift in the palaeo-ITCZ from an Atlantica-concentric monsoon to a zonal-equatorial circulation is associated with the early fragmentation of Gondwana and the disruption of the large low-pressure cell which existed during the summer in the southern hemisphere. This disruption reduced the cross-equatorial pressure gradient between the northern and southern hemispheres and enhanced the Coriolis Effect (Scherer et al., 2020).

The establishment of Cretaceous Hadley cell driven ITCZ played a vital role in the transportation of moisture over tropical regions of NW Africa (Fig. 3 C, D). The moisture is transported via geostrophic winds known as the West African westerly jet - WAWJ (Pu and Cook, 2010). The WAWJ is located within a region of strong westerlies, which is generated by the superposition of the Atlantic ITCZ and the westward expansion of a continental low-pressure cell (Pu and Cook, 2010). A geostrophic wind is produced where opposing coastal pressure cells exist; a "thermal" low-pressure cell resides over the coastal landmass due to the preferential heating of the continental surface relative to slower ocean heating (Bakun et al., 2010). Geostrophic winds can be exacerbated during greenhouse conditions; as the build-up of greenhouse gases in the atmosphere reduces the night-time cooling of the continental landmass, increasing the intensity of the "thermal" coastal low-pressure cell (Bakun et al., 2010).

2.4. Carbon dioxide

The Cretaceous period records a gradual but significant elevation in global mean temperature. The Early Cretaceous (Berriasian, 145 Ma) climate was already a warm 20 °C (average air temperature) having gradually increased since the Jurassic/Early Cretaceous cool period (Scotese, 2004). The global temperatures continued to elevate over the next ~45 Ma, peaking at ~24 °C in the Cenomanian-Turonian during the culmination of the CTM, which translated to tropical sea-surface temperatures of >33 °C (Poulsen et al., 2013) or potentially as high as 42 °C in the equatorial region of the Demerara Rise (Hay & Floegal et al., 2012). This gradual increase in temperature leading up to the CTM has been attributed to outgassing of volcanic CO_2 (Poulsen et al., 2013). Mid-ocean ridge lengths doubled from ~40,000 km in the Jurassic to ~80,000 km in the Early Cretaceous suggesting accelerated seafloor rifting during the breakup of Pangea (Müller and Dutkiewicz, 2018, Fig. 2). Seafloor spreading rates were ~3 cm/year faster during the Jurassic and Early Cretaceous than they are today, also evidenced by an increase in plate convergence from ~5 to ~10 cm/year (Müller and Dutkiewicz, 2018). This degassing of magmatic CO_2 from MORB represents one of the largest outgassing fluxes at the interface of the shallow-surface and deep-Earth (Le Voyer et al., 2018) and provided a significant contribution to the Earth's exogenic CO_2 reservoir. However, whilst there were multiple magmatic and volcanic events occurring throughout the Cretaceous, CO_2 concentrations were actually on the decline from ~2000 ppm 200Ma to ~500–1000 ppm during the CTM (Fig. 2; Rothman, 2002; David, 2017; Müller and Dutkiewicz, 2018).

2.5. Vegetation

Evolution of equatorial Cretaceous biota corresponds with the model for an antithetical change in climate from Early Cretaceous aridity to mid-Late Cretaceous greenhouse conditions. Palynological studies of West-African basinal sediments by Salard-Cheboldaeff and Dejax (1991) evidence the predominant occurrence of gymnosperms (Kunzmann et al., 2006) which are believed to indicate xeric conditions throughout the very-Early Cretaceous (Barremian-Aptian; Fig. 10 A). During the Late Aptian and Early Albian, a shift to more humid conditions is evidenced by an increased abundance of spores related to aquatic angiosperms (Wang and Dilcher, 2006, Fig. 10 B). Cenomanian microflora is akin to that of the Albian, but with a decrease in fern spores and the progressive replacement of gymnosperms with angiosperms (Salard-Cheboldaeff and Dejax, 1991). During the Turonian, the sudden disappearance of the gymnosperms: Cheirolepidaceae and Proteaceae (Salard-Cheboldaeff and Dejax, 1991) reaffirms the model of increasing humidity during the CTM (Fig. 10 C). The Senonian microflora from Senegal is characterised by an increase in the angiosperms: Graminae and Palmaceae (Salard-Cheboldaeff and Dejax, 1991), suggesting the climate was still hot by modern standards with geostrophic oceanic influence with an established archetypal equatorial forest, dominated by angiosperms. During the Maastrichtian Senegalese macrospores, microspores, massulae related to extent Azolla and Salvinia, and aquatic fern spores indicate similar hot and damp ecological conditions with extensive vegetation found around lakes and swamps (Fig. 10 D).

Cretaceous Thermal Maximum.

What caused the CTM is still debated. Factors could include high concentrations of carbon dioxide in the atmosphere, that frequently associated with periods of climate change, or sea water temperature and distribution of water bodies (shallow seas) covering the continents.

Atmospheric CO_2: Carbon dioxide is frequently ascribed as a contributing factor for the CTM, with estimations varying between <900 and 5000 ppm (summary by Bice and Norris, 2002), but this is debateable. During the mid to upper Cretaceous, atmospheric CO_2 was on the decline (Rothman, 2002; David, 2017; Müller and Dutkiewicz, 2018; Wilson et al., 2002). Haq and Huber (2017) proposed this period of extreme warmth would require high partial pressures of CO_2 in the range of 700–4000 ppm resulting from high rates of volcanic degassing, which were deemed unreasonably excessive. Haq and Huber (2017) also suggest that elevated levels of methane may at least be partially responsible for the CTM, as methane is a 10 times more potent greenhouse gas than CO_2. Poulsen et al. (2013) determines an association between geological observations and climate model simulations to support their hypothesis that the CTM was at least partly a climatic expression of tectonically driven oceanographic events.

Distribution of water bodies (shallow seas): Shallow seas covered many of the continental landmasses during the Mid-Cretaceous, markedly different from today, with an estimated 20% less land-surface (Hay et al., 2019). Heimhofer et al. (2018) attributed accelerated hydrological cycling and enhanced weathering to a generally more humid climate. Increased humidity as a potential contributing cause for the CTM is a plausible hypothesis given the increased sea-level and associated oceanic surface-area. The combined increase in oceanic surface-area and expanded ITCZ could have intensified evapotranspiration increasing global temperatures and humidity, causing a hydrological positive feedback loop. This positive feedback loop would have increased further through expansion of vegetation to higher latitudes.

Water vapor as a contributing factor to the CTM: Increased precipitation and associated humidity has strong potential for water vapor being a reasonable candidate as a contributing factor for the CTM. Whilst there is no precise data for precipitation rates during the CTM, estimates of Late Cretaceous precipitation by Sellwood and Valdes (2006) suggest up to and possibly over 5840 mm/year in Senegal.

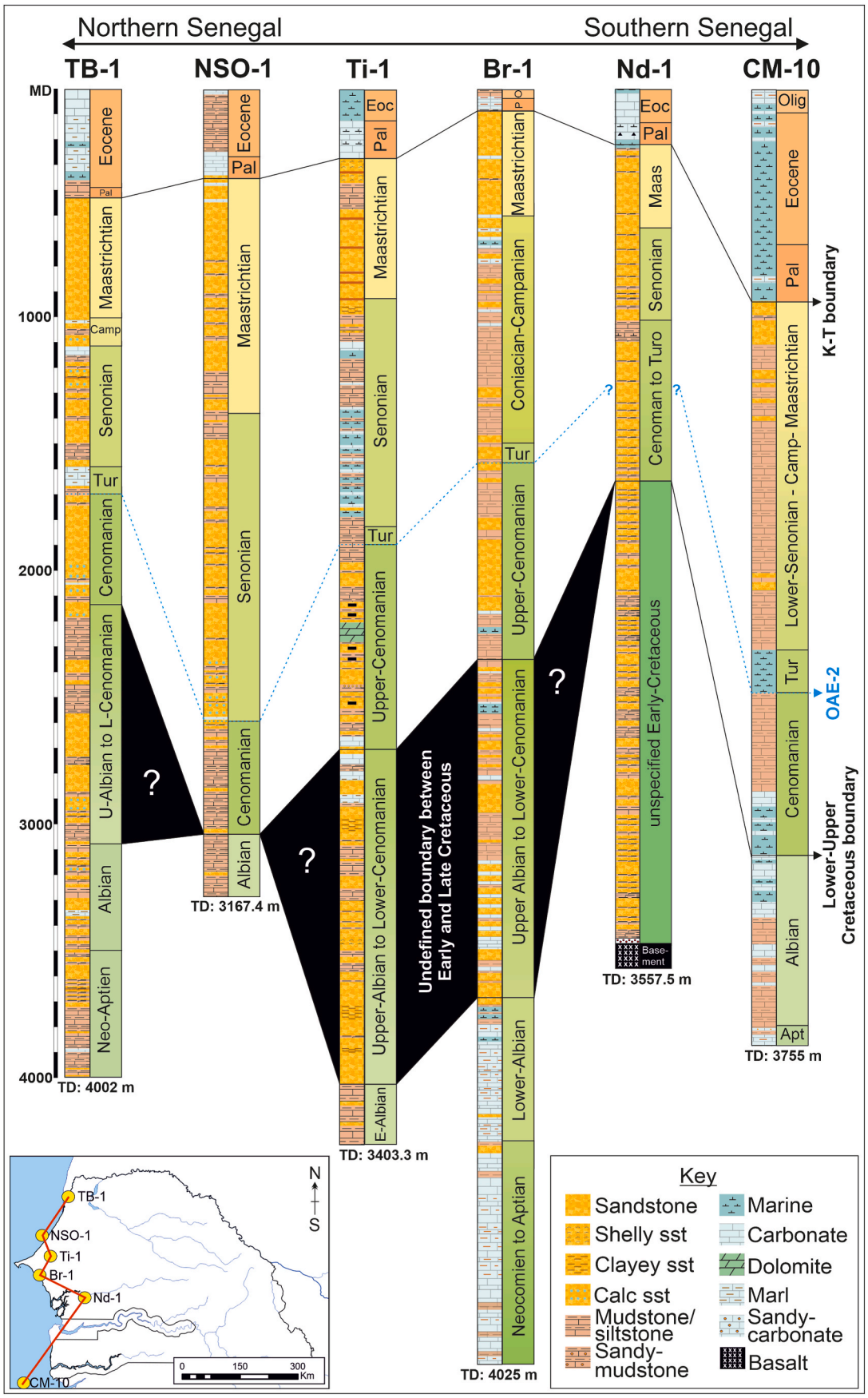

Fig. 4. Synthetic chronostratigraphic summary of key nearshore Senegalese exploration wells, including a basic geological map displaying proximal Precambrian terranes. Mid-Cretaceous boundary for wells TB-1, Ti-1, Br-1 and Nd-1 are undefined.

Infra-red radiative absorption of water vapor occurs at multiple wavelengths making water vapor a very potent greenhouse gas, whereas absorption by CO_2 is limited to three main bands at 2.7, 4.3, and 15 nm (Held and Soden, 2000; Pierrehumbert, 2002; Anderson et al., 2016).

Ocean Circulation: The juvenile EAG was relatively shallow and together with potentially reduced Atlantic-Pacific Ocean circulation due to the emplacement of the Caribbean LIP could have resulted in restrictions in oceanic circulation. This would have prohibited global thermohaline regulation. (Figs. 2 and 3).

The decline of the CTM and a return to lower global temperatures may have been a gradual process as an atmospheric and oceanic equilibrium was reached through prolonged and exceptional carbon sequestration through photosynthesis and increased silicate weathering. This coincided with the establishment of the deeper-marine EAG (Pérez-Díaz and Eagles, 2017) allowing the comparably fresher waters of the southern Atlantic Ocean to enter into the hypersaline northern Atlantic Ocean. This oceanographic halokinetic-type circulation may have allowed for the transfer of heat around the Earth via a proto-Gulf Stream (Hay, 2009; Pérez-Díaz and Eagles, 2017; Poulsen et al., 2013).

3. Materials and methods

3.1. Data collection

DSDP mudstone cuttings from wells 367 and 368 were obtained from the DSDP core repository, University of Bremen, Germany (sample collection request identification: 054376IODP, 065859IODP and 077865IODP) and cuttings from nearshore wells: CM-10, Ti-1, NSO-1 and TB-1 were collected from the Petrosen core-repository (Dakar, Senegal). Clay-mineralogical data for DSDP 534 is extracted from Chamley et al. (1983). Bulk-rock and clay-mineralogical data for KaF-1 is extracted from Chamley et al. (1988). Isotopic data for CM-1 and DSDP wells 367 and 368 is extracted from Mourlot et al. (2018[2]). Mineralogical and isotopic analyses were conducted at the British Geological Survey, Nottingham, UK.

3.2. Sample preparation

Samples were subdivided for bulk-rock X-ray diffraction (XRD) and orientated-clay XRD. The aliquot for bulk-rock XRD was milled to a coarse (125 μm) powder. In order to provide a finer and uniform particle-size for bulk-rock XRD analysis, a 0.9g portion of each milled sample was micronised under acetone for 10 min with 10% (0.1g) corundum (American Elements - PN:AL-OY-03-P). The addition of an internal standard allows the validation of quantification results.

For orientated-clay mineralogy the remaining crushed sample was dispersed in distilled water using a reciprocal shaker combined with ultrasound treatment. The suspensions were then sieved on 63 μm ('sand') and the <63 μm material placed in a measuring cylinder and allowed to stand. In order to disperse the individual clay particles and prevent flocculation, 1 ml of 0.1M sodium hexametaphosphate was added to each suspension. A nominal <2 μm ('clay') fraction was removed after a settling period of 16 h.

Approximately 70 mg of the <2 μm material was re-suspended in distilled water and pipetted onto a ceramic tile in a vacuum apparatus to produce an oriented mount. The mounts were Ca-saturated using 0.1M $CaCl_2{\cdot}_6H_2O$ solution, washed twice to remove excess reagent and air-dried overnight.

3.3. X-ray diffraction analysis

XRD analysis was conducted using a PANalytical X'Pert Pro series diffractometer equipped with a cobalt-target tube, X'Celerator detector and operated at 45 kV and 40 mA. The micronised powder samples were scanned from 4.5 to 85°2θ at 2.06°2θ/minute. Diffraction data were initially analysed using PANalytical X'Pert HighScore Plus version 4.9 software coupled to the latest version of the International Centre for Diffraction Data (ICDD) database. Following identification of the mineral species present in the samples, mineral quantification was achieved using the Rietveld refinement technique using SiroQuant v4 software.

The <2 μm oriented mounts were scanned from 2 to 40°2 θ at 1.02°2 θ/minute after air-drying, after glycol-solvation and after heating to 550 °C for 2 h. Clay mineral quantification was achieved using the method defined by Biscaye (1965). The <2 μm fraction is chosen because of the reasonable assumption that 100% of the mineralogy is constituted by chlorite, illite, kaolinite and smectite (Biscaye, 1965).

3.4. Nd/Sr isotopic analysis

Preparation of samples for Nd/Sr isotopic analyses are based upon the parameters defined by Bird et al. (2020). Nd fractions were dissolved in 1 ml of 2% prior to analysis on a Thermo Scientific Neptune Plus mass spectrometer operated in static multicollection mode. Data are normalised to $^{146}Nd/^{144}Nd = 0.7219$. Twenty-six analyses of the JNd-i standard gave a value of 0.512071 ± 0.000008 (1-sigma). Results are quoted relative to a value of 0.512115 for this standard. Two analyses of the BCR-2 rock standard run with the samples gave identical results of 0.512633 ± 0.000003 (1-sigma).

Sr fractions were loaded onto outgassed single Re filaments using a TaO activator solution and analysed in a Thermo-Electron Triton mass spectrometer in multi-dynamic mode. Data are normalised to $^{86}Sr/^{88}Sr = 0.1194$. Six analyses of the NBS987 standard gave a value of 0.710267 ± 0.000004 (1-sigma). Sample data is normalised using a preferred value of 0.710250 for this standard. Two analyses of the BCR-2 rock standard run with the samples gave a value of 0.705014 ± 0.000010 (1-sigma).

4. Results

4.1. Nearshore well mineralogy (Fig. 7)

4.1.1. TB-1

Samples collected from well TB-1 from the Aptian and Albian interval are predominantly quartz-rich sandstones with a moderate feldspar and K-feldspar content. Carbonate content increases from the Cenomanian-Turonian transition and into the Campanian, where carbonate content is equivalent to quartz content. The clay-mineralogy during the Aptian and Albian is predominantly illite and chlorite with subordinate kaolinite. Illite is the dominant clay in the Aptian, with chlorite the main component in the Albian. Chlorite is absent in the Upper Cretaceous, substituted by kaolinite as the dominant clay. Smectite occurs throughout the Cenomanian-Turonian transition and into the Santonian. The clay-mineralogy of TB-1 in the Campanian is almost entirely illite based with very little kaolinite.

4.1.2. NSO-1

Albian to Cenomanian samples include mixed argillaceous (30–40% quartz, feldspar and K-feldspar) mudstones, changing to argillaceous carbonate mudstones (marls). The clay-mineralogy is dominated by illite between the Albian and Early-Turonian with moderate kaolinite and subordinate chlorite and smectite. Kaolinite and smectite content increases during the Late-Turonian becoming the dominant clays through to the Lower-Maastrichtian. Chlorite appears again during the Mid-Campanian. A single sample towards the end of the Maastrichtian is predominantly chloritic with subordinate illite.

4.1.3. Br-1

There is a sharp mineralogical break between the Early-Aptian and Early-Albian sediments, reflecting the transition from sandstone to carbonate. With a lack of Mid-Aptian data, it is unclear precisely when this transition occurred. Sampled Albian to Coniacian sediments include sandstone to argillaceous-sandstone. Clay mineralogy is predominantly

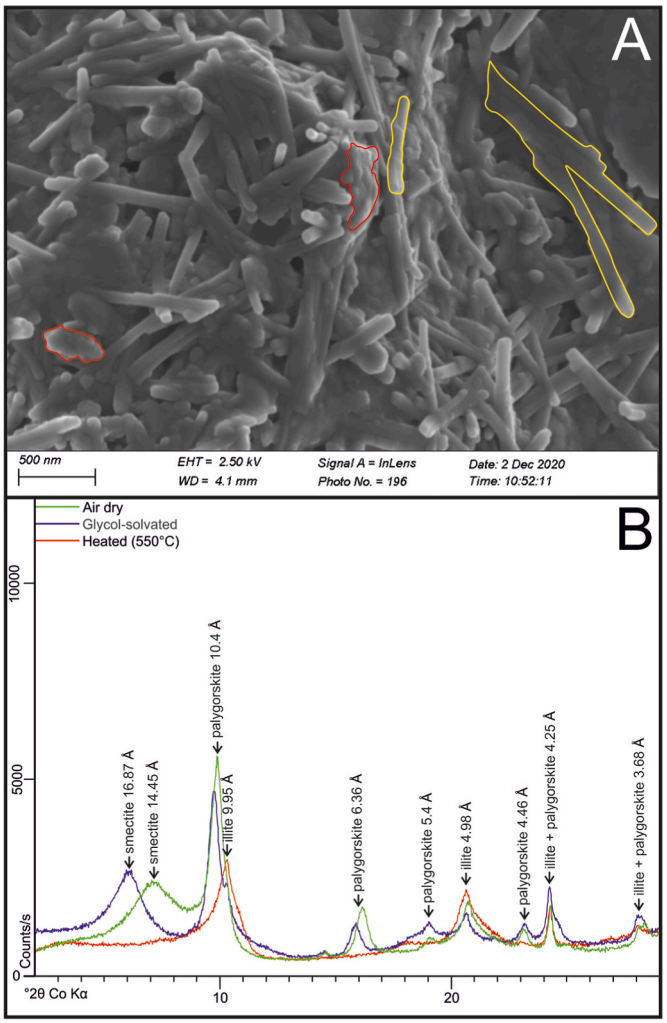

Fig. 5. A, BSE-imaging of palygorskite rods (highlighted in yellow) interspersed amongst fine-grained smectite (highlighted in red). B, <2 μm orientated clay X-ray diffraction scan showing principle low-angle palygorskite peaks.

illitic throughout the Early-Cretaceous with increasing kaolinite and chlorite throughout the CTM peaking during the OAE2 at the Cenomanian-Turonian transition.

4.1.4. Ti-1

The Albian to Upper-Cenomanian interval consists of variegated sandstones, siltstones and marls before transitioning to argillaceous carbonate mudstones from the Turonian to the Lower-Maastrichtian. The clay-mineral assemblage is illite dominant in the Albian to Upper-Cenomanian with variable subordinate chlorite and kaolinite. The clay-mineral assemblage changes abruptly at the Cenomanian-Turonian transition becoming kaolinite and smectite dominant with subordinate illite.

4.1.5. Nd-1

Samples collected from Nd-1 are predominantly quartz-rich sandstones with moderate feldspar and K-feldspar content in the Aptian and Albian, with a minor occurrence of carbonate appearing in the Cenomanian. The clay-mineral assemblage contains broadly comparable amounts of kaolinite, chlorite and illite until the Cenomanian-Turonian transition; when the clay-mineral assemblage changes abruptly to a kaolinite and smectite dominant assemblage with subordinate illite.

4.1.6. KaF-1

Between the Valaginian and Cenomanian KaF-1 comprises sequences of marly-sandstones and mudstones transitioning into limestones. On average they contain up to 50% calcite with variations in associative quartz and clay content. The Late Cenomanian to Maastrichtian interval consists of mudstones and claystones at the base, transitioning into sandstones during the Maastrichtian, recognised by a progressive increase of quartz and clays and reduction in carbonate. The Paleogene is characterised by platform carbonate deposits with minimal clay content and little quartz. The Miocene shows a shift from the Paleogene carbonates to sandstones and mudstones. The clay mineralogy of well KaF-1 can be subdivided into four mineralogical intervals: 1, Valaginian to Early Aptian is characterised by abundant chlorite (30–70%) and illite (20–50%) with a minor mixed layer component and trace quantities of kaolin. 2, Middle Aptian to Late Cenomanian is characterised by a gradual reduction in chlorite and illite content and a gradual increase in kaolin. Towards the end of the Cenomanian there is a sudden increase in kaolin with a corresponding increase in smectite content. 3, Late Cenomanian to the end of the Maastrichtian epoch shows a gradual increase in smectite to become the dominant clay-mineral. 4, Palaeocene to Miocene is marked by a noticeable increase in palygorskite and associated sepiolite.

4.1.7. CM-2

Samples are restricted to the Paleogene interval and comprise sandstones with varying proportions of carbonate, gypsum and pyrite. Clay mineralogy is predominantly kaolinitic with trace quantities of illite.

4.1.8. CM-4

Sampled sediments from CM-4 comprise of argillaceous-quartz rich marl with varying proportions of carbonate during the Early-Cretaceous before transitioning to quartz-dominated sandstones during the Cenomanian. The uppermost sample of CM-4 returns to a carbonate dominated mineralogy at the Cenomanian-Turonian transition.

4.1.9. CM-10

Aptian to Late-Cenomanian samples comprise of argillaceous carbonate mudstones but unlike the other Lower-Cretaceous deposits CM-10 is devoid of K-feldspar and includes the infrequent occurrence of the clinopyroxene pigeonite ((Mg, Fe^{2+}, Ca) (Mg, Fe^{2+}) Si_2O_6). Carbonate content diminishes in the Coniacian and Santonian transitioning to silica-rich argillaceous mudstones, until the Campanian with the reoccurrence of carbonate, which increases substantially during the Maastrichtian. The clay-mineralogy can be subdivided into three units, the first is illite dominant with subordinate kaolinite and chlorite extending from the Aptian to the Upper-Albian. The second unit encompasses the Cenomanian epoch and is illite dominant with subordinate kaolinite. The third unit begins at the Cenomanian-Turonian transition and exhibit a sudden change in clay-mineralogy with a sudden increase in kaolinite and the introduction of smectite into the clay-mineral assemblage. The unit in kaolinite dominant in the Turonian but transitions to a smectite dominant assemblage in the Upper-Campanian and Maastrichtian.

4.1.10. NCF-1

The lowermost two samples are designated lower and upper Senonian (which accounts for Coniacian to Campanian and possibly Maastrichtian) and the uppermost sample is Maastrichtian age. All three samples are comprised of sandstone with a marginal carbonate increase in the Maastrichtian. Lower Senonian (Coniacian to Mid-Campanian?) clay mineralogy is predominantly illitic with chlorite and trace kaolinite, this transitions to a kaolinite dominated clay-mineral assemblage during the Upper-Senonian (Campanian to Maastrichtian) with minor illite and smectite. By the Maastrichtian, kaolinite remains the dominant clay mineral with a minor increase in smectite and an absence of illite.

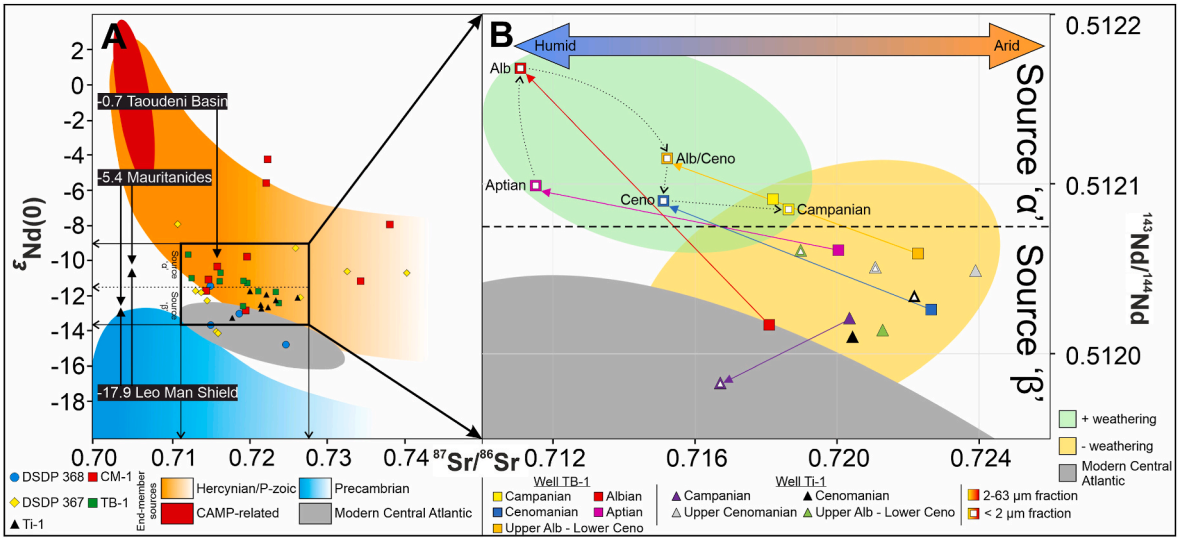

Fig. 6. A, Cross plots of εNd (0) and $^{87}Sr/^{86}Sr$ values, DSDP367, 368 and CM-1 taken from Mourlot et al. (2018[2]) and TB-1 and Ti-1 from this study. Highlighted in black are average εNd (0) values for the three most proximal NW-African sources to the MSGBC Basin (Taoudeni Basin, Mauritanides and Leo Man Shield) established by Mourlot et al. (2018[2]). B, Magnification of Fig. 6A; $^{143}Nd/^{144}Nd$ and $^{87}Sr/^{86}Sr$ values for samples from TB-1 and Ti-1 including < 2 μm and 2–63 μm fractions, "orange" Hercynian/Palaeozoic source divided into source α (green) and source β (yellow).

4.1.11. DM-1

The core from well DM-1 contains the oldest sampled sediment in this study (Silurian and Devonian), both are quartz-arenite sandstones (99%), trace quantities of clay (<0.5 %) is predominantly kaolinitic which is likely authigenic in origin.

4.1.12. DSDP 534

DSDP 534 samples can be assigned to defined formations. They include: Plantagenet Fm. (Maastrichtian), variegated claystones. Hatteras Fm. (Cenomanian-Upper Barremian), black to green carbonaceous claystones. Blake-Bahama Fm (Barremian-Berriasian), bioturbated & laminated limestones and chalk grading upwards into calcareous and carbonaceous claystones, re-sedimented shelf limestones and quartzose siltstones (Chamley et al., 1983). The clay-mineralogy is predominantly comprised of terrigenous-derived smectite (Chamley et al., 1983). The clay-mineralogy remains proportionally similar throughout most of the Cretaceous with a few intermittent increases in illite content occurring throughout the Aptian, Albian and Maastrichtian, these peaks also include progressive increases in kaolin content especially during the Maastrichtian. Occurrence of palygorskite is recorded throughout DSDP 534 but is more prominent in the Plantagenet Fm. (Upper-Campanian to Maastrichtian).

4.1.13. DSDP 367

DSDP 367 (Cap Verde Basin; Casson, 2020c) is the southernmost offshore well and is comparatively closer to the coastline of Senegal than DSDP368. Units 5b and 5a (Berriasian to Lower Aptian) contain predominantly argillaceous limestones and calcareous marls. Units 4b, 4a and 3 (Albian to Santonian) consists of argillaceous mudstones with carbonate-rich mudstones occurring throughout the Albian and Cenomanian. Lower-Unit 3 (Cenomanian-Turonian transition) is notable by the occurrence of palygorskite (28.3% bulk-rock mineralogy). Due to the fibrous/rod-like structure of palygorskite (Fig. 5 B), it can be difficult to quantify its occurrence amongst the other "platy" clays which are typically quantified using orientated <2 μm clay mounts (Kemp et al., 2016: Fig. 5 A) therefore palygorskite content is only depicted within the bulk-rock mineralogy. Units 5B and 5A (Berriasian to Lower-Aptian) clay-mineralogy is predominantly illite and smectite with trace quantities of kaolinite during the Valanginian and Hauterivian. Kaolinite content increases in Unit 4A (Upper-Albian to Lower-Cenomanian), returning to a smectitic assemblage in Unit 3 (Turonian to Coniacian).

4.1.14. DSDP 368

DSDP 368 (Lamont-Doherty and Bukry, 1978a[b]; Casson, 2020c[c]) is located on the south-western margin of the Cap Verde Rise is located approximately 580 km NNW of site 367. DSDP sediments consist of thick hemipelagic facies which are characteristic of continental margin deposition. Unit 3 consists of black shales and diabase sills, Unit 2C contain cyclic interbeds of green silty-clay and mudstone and Site 2B containing interbedded green and red mudstone (Chamley et al., 1988). The cyclic red and green mudstones of Unit 2b have been associated with fluctuating redox conditions, analogous to those of site 367 (Chamley et al., 1988). Carbonate is restricted to two samples of Late-Cenomanian and Mid-Campanian age, the near-complete absence of carbonate was noted by Chamley (368 log). The clay-mineralogy during the Turonian marks the only occurrence of chlorite. The Coniacian and Upper-Campanian to Maastrichtian epochs contain similar clay assemblages with near-equal amounts of illite, smectite and kaolinite, this is divided by a predominantly illite and smectite assemblage during the Santonian and Lower Campanian. Palygorskite occurrence is more frequent in DSDP368 than 367, which deposits observed in the Turonian, Santonian and Campanian epochs.

4.1.15. Maastrichtian coastal outcrops

The section that outcrops at Cap de Naze (Table 1; Fig. 9) is comparatively enriched in quartz compared with Maastrichtian section at Cap Rouge (Table 1; Fig. 9), which has a greater clay component plus halite, goethite and hematite (other: 4.6%). There is however, a very good agreement between the clay mineralogy, whereby kaolinite is the dominant clay (73–74%) and illite (24–28%). For reference, the average clay-mineral composition of both Cap Rouge and Cap de Naze is used in Fig. 11.

4.1.16. Nd/Sr isotopes

Strontium (Sr) and Neodymium (Nd) isotopes are an extremely useful geochemical tool for provenancing terrigenous sediments that reflect major changes climate-based weathering rates (Meyer et al., 2011; Bretschneider et al., 2021; Mourlot et al., 2018b). Nd is used as a reliable indicator for the sedimentary provenance, as these isotopes are more resistant to fractionation through near-surface processes such as

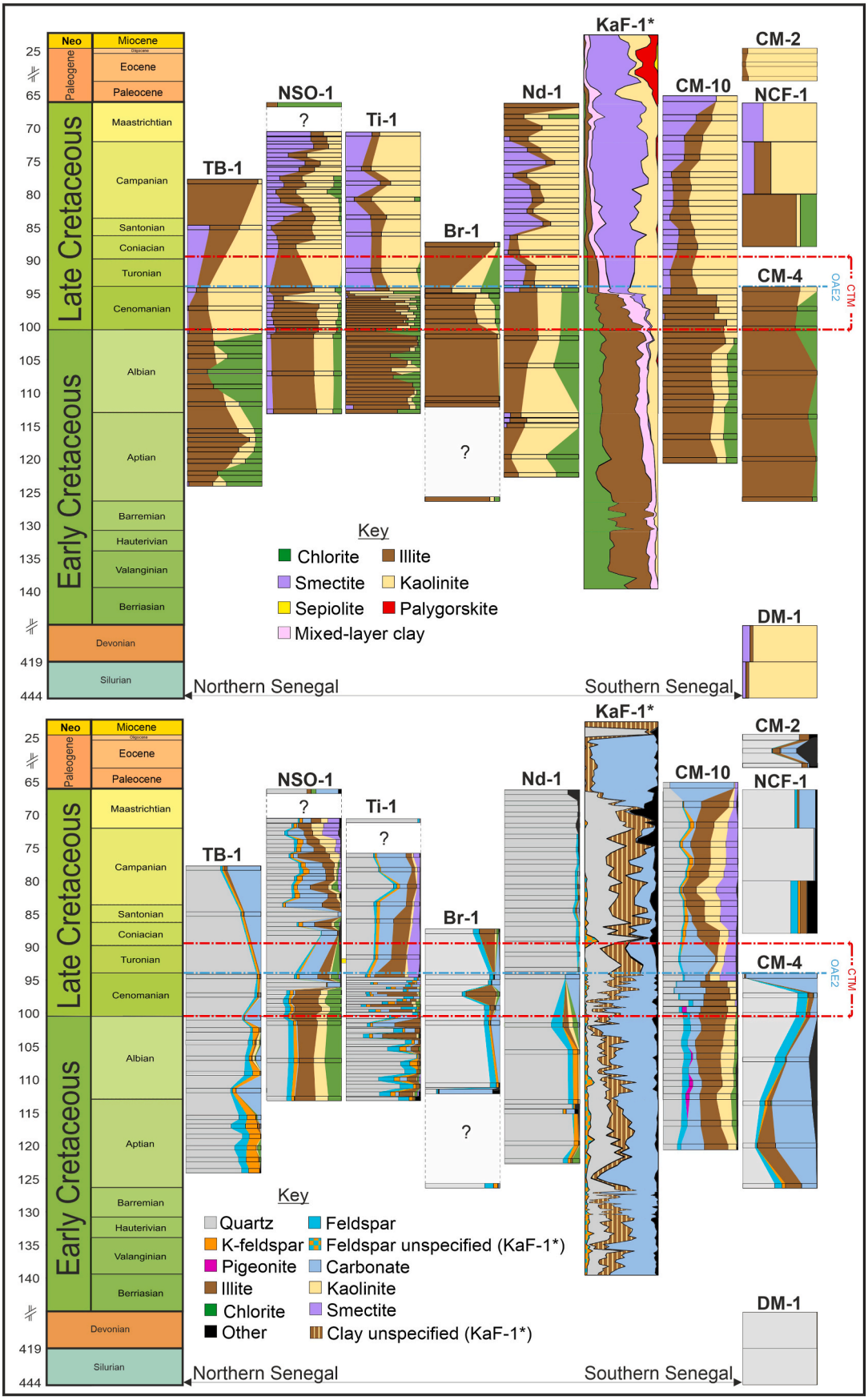

Fig. 7. Clay mineralogy (Upper) and bulk rock mineralogy (lower) for nearshore wells. KaF-1* data extracted from Chamley et al. (1988).

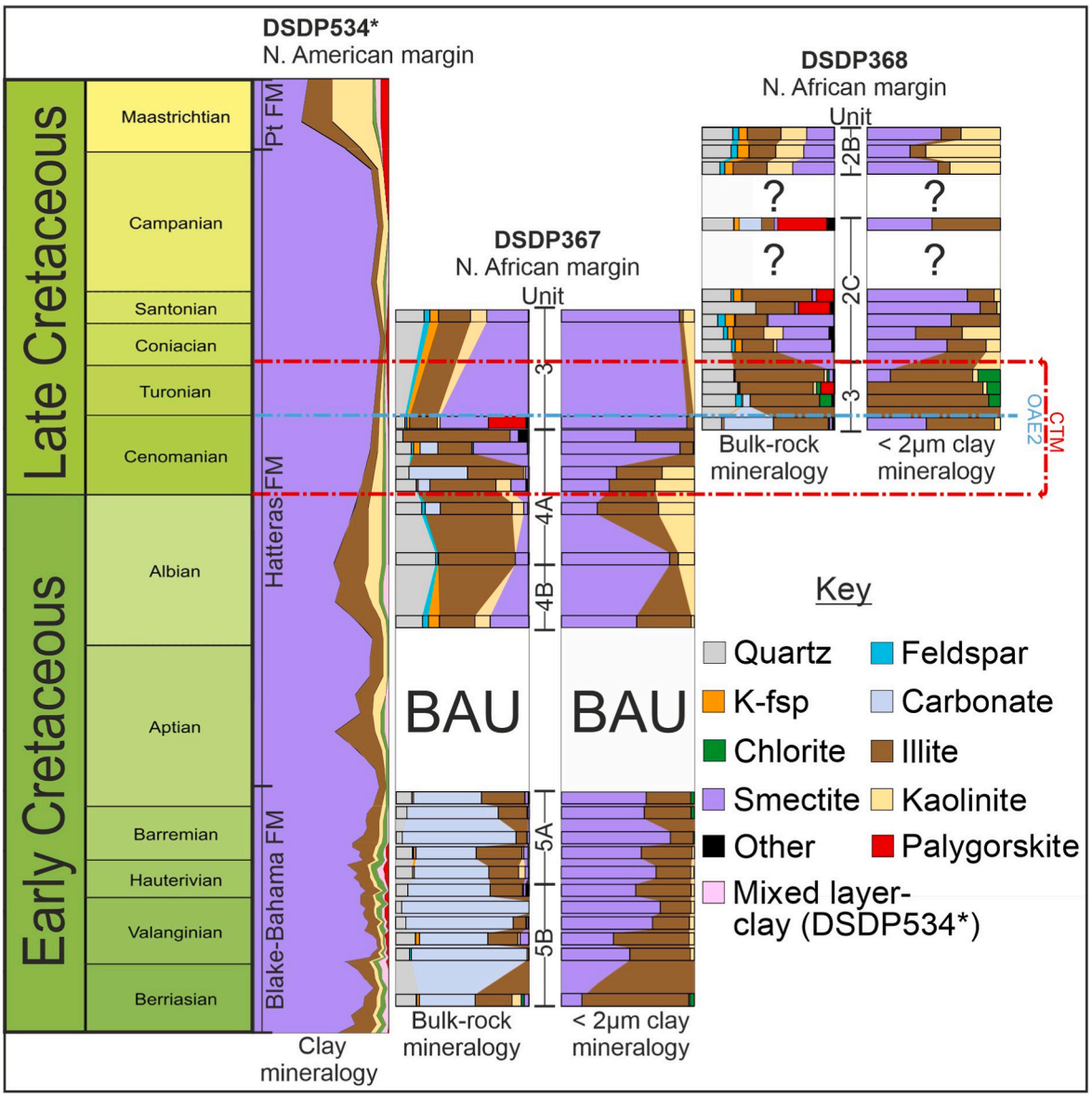

Fig. 8. Bulk rock and clay mineralogy by XRD for DSDP wells, DSDP534* data extracted from Chamley et al. (1983). Pt FM (Plantagenet Formation), BAU (Base Albian Unconformity).

chemical weathering. Alternatively, Sr is far more mobile during chemical weathering and can be readily eluted from the clays. However non-weathered clays are typically enriched in radiogenic Sr because of the preferential radioactive decay of Rb, common in phyllosilicates.

In this study εNd (0) TB-1 and Ti-1 isotopic values range between −9 and −13 epsilon and $^{87}Sr/^{86}Sr$ values range between 7.11 and 7.24, corresponding with the isotopic end-member Hercynian/Palaeozoic source (Fig. 6 A) established by Mourlot et al. (2018[2]) with the minor exception of < 2 μm fraction of Ti-1 Campanian sediment which plots within the Modern Central Atlantic source with an εNd (0) value of −12.78. Aptian to Cenomanian clay and Campanian clay + silt have comparably higher radiogenic Nd compared to the remaining TB-1 silt and Ti-1 fractions (Fig. 6 B) and are designated as source alpha (α) and beta (β respectively) based on their associated Nd values.

5. Discussion

5.1. Deep sea mineralogy

Early Cretaceous sediments from DSDP wells 534, 367 and 368 are predominantly comprised of smectite. The origin of the smectite could be detrital or diagenetic. If detrital, this can be associated with aridity, sparse plant-cover and reduced chemical-weathering which provides optimal conditions to facilitate the generation of terrestrial smectites. Mounteney et al. (2021) addressed the potential provenance of sediments to the 367 and 368 locations, interpreting sediment input from weathered Si-poor lithologies from high-altitude regions of the West African Craton (WAC). In Chamley et al. (1988), they interpreted samples from KaF-1 and DSDP 367 as containing a deep-sea smectite component from a terrigenous supply, derived from poorly drained soils from within the WAC hinterlands. REE analysis of NW African DSDP 367, 368, 369, 415A, 370, 416, and 138 sediments by Mourlot et al. (2018[2]) reaffirms an interpretation of a detrital origin for the smectite,

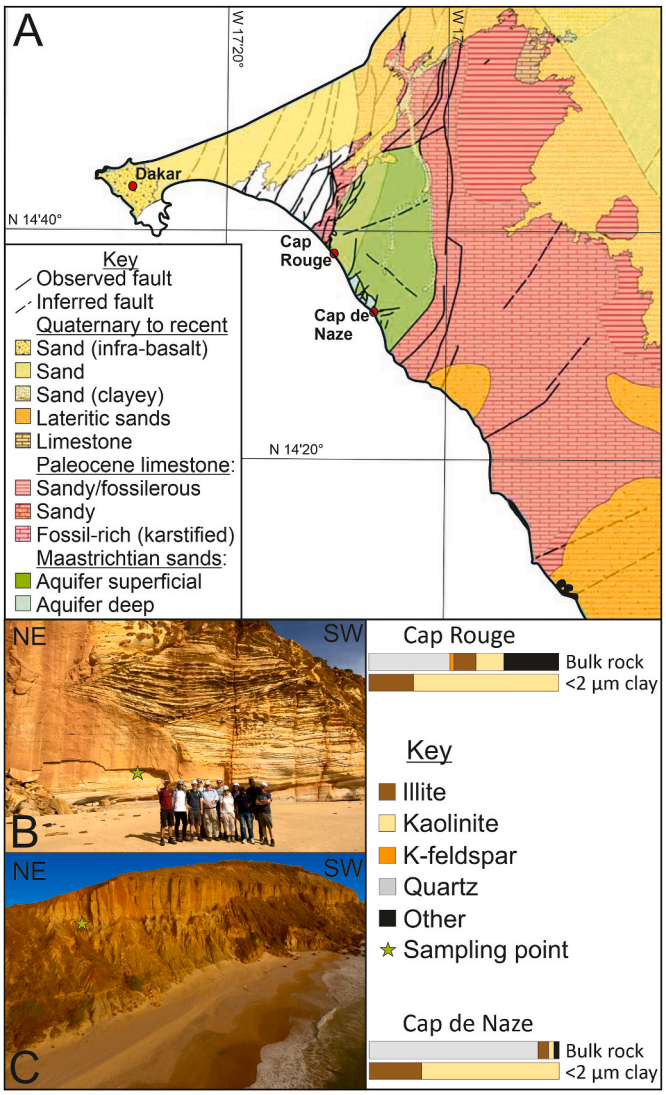

Fig. 9. A, Geological map of western Senegal (M'bour region) modified from Barusseau et al. (2009). B, Cap Rouge exposure and associated bulk rock and <2 µm clay mineralogy. C, Cap de Naze exposure and associated bulk rock and <2 µm clay mineralogy.

as they possess Ce anomalies higher than or equal to 0.66. This indicates that even if some of the smectites were authigenic, were formed during early diagenetic processes, their proportion would very likely still be significantly less than the detrital fraction. Mourlot et al., (2018a) also noted that sediments from DSDP and CM1 had higher Cr/Th ratio, but lower Th/Sc values and Eu anomalies when compared to the Post Archean Australian Shales (PAAS; Taylor and McLennan, 1985), suggestive that these detrital sediments were sourced from less differentiated sources than those of PAAS, with the latter considered as archetypal upper continental-crust. Smectite broadly remains the dominant clay species in the DSDP well sediments throughout the Cretaceous (Fig. 8), yet smectite in the neritic/onshore wells does not occur in any abundance until the Cenomanian/Turonian, which corresponds with the peak CTM and OAE2.

Two significant occurrences of kaolinite are observed in the Albian to Lower-Cenomanian interval in DSDP 367 and Upper-Campanian to Maastrichtian interval in DSDP 368. These occurrences correlate with kaolinite deposits on the western margin of the Atlantic Basin at DSDP 534 suggesting basin-wide shifts in climate from arid to humid between the palaeo-latitudes of ~N10° and ~N30°. Units 5B and 5A of DSDP 367 (Berriasian to Lower-Aptian) is highlighted by the occurrence of argillaceous limestones and calcareous marls noted by Chamley et al. (1988), which are calcitic in nature. Further calcitic-carbonate also occurs throughout the Cenomanian (DSDP367 and 368). The carbonate encountered the Mid-Campanian in DSDP 368 is dolomitised (9.2% dolomite, 7.3% ankerite and 0.4% siderite). The formation of magnesian and ferroan-dolomite requires sufficient Mg and Fe ions for dolomitisation to occur. Seawater is overwhelmingly the most abundant Mg-bearing fluid available, however, elevated temperatures are required for dolomitisation to occur.

The presence of concentrated oceanic brines is interpreted to be the result of low-latitude marginal shallow seas, where ion concentration was exacerbated through increased evaporation and the erosion of older NW African evaporites fed from the Saharan platform. These brines were eventually transported down the continental slope to form Warm Saline Bottom Waters (WSBW; Brass et al., 1982. However, these Mg-rich WSBW's are not solely responsible for the production of palygorskite, increased silica is also required. A probable source for this increased silica is from biogenic sources, in particular radiolarians, which are frequently preserved in the Western Atlantic (Brosse, 1982) and the deposition of thick black shales on the Eastern side of the Atlantic (Graciansky et al., 1987) both inferring exceptionally high organic productivity. In this scenario, the Eastern Atlantic palygorskite and palygorskite-dolomite paragenesis reflect Mg and Si rich environments (Thiry and Pletsch, 2011). Accelerated deposition of biogenic silica can be linked with periods of ocean anoxia and marine extinction, which was frequent during the Cretaceous greenhouse periods via several punctuating oceanic anoxia events. Indeed, the occurrence of palygorskite in DSDP 367 corresponds precisely with the Cenomanian/Turonian transition and the OAE2 interval, the Turonian palygorskite of DSDP368 resides chronologically above the OAE2 but is still within the timeframe of the CTM event. The Santonian and Campanian palygorskite of DSDP 368 may correspond with the regional extent of OAE3, but this is conjecture as OAE3 is poorly constrained. This Late Cretaceous palygorskite may be linked to the beginning of the Cape Verde volcanism (Fig. 11 E). If palygorskite is a reliable proxy for ocean anoxia, its suggests that OAE3 may have occurred as two stages; OAE3A (Santonian) and OAE3B Campanian, restricted to the Northwest African Atlantic Margin (NWAAM). A sedimentary hiatus commonly referred to as the base Albian unconformity (Casson, 2020c[c]) is believed to have occurred at the end of the Aptian, observed at DSDP 367 (Fig. 8), Chamley et al. (1988), and it is proposed that this hiatus resulted from the tectonic reaction of continental margins to an accelerated stage of ocean spreading.

5.2. Nearshore mineralogy

The Valanginian interval in DSDP 367 contains clays that include illite and smectite, whereas the corresponding interval in the well KaF-1 contains predominantly chloritic clays. In a typical coastal depositional setting, grain-size mineralogical bias is expected, whereby finer grained clays would be transported further offshore, whilst coarser grained clays would be deposited within the continental slope/shelf transitional zone. This may explain the preferential abundance of chlorite in KaF-1 but not why KaF-1 is devoid of smectite, which may infer different lithological sources and mode of transportation during the Valanginian.

The Late Jurassic to Early Cretaceous climate of NW Africa, based on a variety of published evidence and our observations, was subject to arid conditions. This resulted in development of only minor probably ephemeral fluvial systems. This would have coincided with the optimal conditions for the development of high-altitude smectite formation. This smectite would have been the transported offshore and recorded in sediments in the DSDP wells and the Mid-Late Cretaceous sediments sampled from the nearshore wells. Early Cretaceous tropical continental air mass winds, and the change to NE-SE trade winds in the Valanginian-Barremian, would have been the principal method of transport by which smectite and illite were transported from the onshore Cretaceous-WAC

Fig. 10. Portrayal of river-systems and representative ecosystems for Senegal during the Cretaceous: A, Berriasian to Barremian (Schimmeck, 2021). B, Aptian (Curioso Photography, 2020). C, Cenomanian to Turonian (Grossenbacher, 2022) and D, Maastrichtian (Bouchouicha, 2022).

into the proto-North Atlantic marine basin. Present day aeolian-dust, recovered from equatorial North Atlantic deep marine sediments, have been used by Moreno et al. (2001) and Stuut et al. (2005) to reconstruct palaeoenvironmental changes in NW Africa. Aerosol sediment traps located offshore Senegal and Cape Verde have revealed NW Africa aerosol-sedimentation rates of a few mm/yr (Stuut et al., 2005). Total Ozone Mapping Spectrometry (TOMS) of airborne dust-particles (Stuut et al., 2005) show large swathes of NW Africa and the surrounding Atlantic Ocean that contain elevated levels of airborne silt and clay. In the Early Cretaceous, our model suggests offshore smectite/illite is transported by tropical continental air mass winds and later the subsequent NE-SE trade winds, whilst illite and chlorite may have been fluvially derived from a source to the south of Senegal.

All neritic clay-mineralogy in the Early Cretaceous is predominantly inclusive of illite and chlorite, with minor kaolinite, in all intervals sampled with exception to samples from well Nd-1, which has an increased kaolinite content. The occurrence of illite and chlorite is associated with the physical weathering of low-grade metamorphic lithologies with minimal chemical weathering, as expected in an arid climate (Akinlotan et al., 2022). During the Early-Mid Cretaceous, deposits traversed by Nd-1 were the most easterly (inner-shore) and the occurrence of kaolinite is probably representative of a local kaolinitised source which could be diagnostic a transition to a more humid climate. This increase in kaolinite continued into the Late Cretaceous inferring a continuation of NW African humidity.

Chamley et al. (1988) identified the pronounced mineralogical shift between Lower Cretaceous chlorite and Upper Cretaceous Smectite in KaF-1 and determined that "such a strong mineralogical break is unknown in sedimentary series marked by normal argillaceous diagenesis due to increased depths and age". This mineralogical break also includes a significant increase in kaolinite occurring at varying intervals between the Cenomanian and Turonian, coinciding within the timeframe of the CTM. The associated increase in humidity is reflected within the Upper Limit of the Equatorial Humid Zone (Figs. 3 and 11) and it is this increased humidity and temperature which probably generated larger NW African river systems, with catchments potentially extending deeper into the hinterland to include the western interior of the WAC and the northern limits of the Leo Man Shield. These evolved fluvial catchments eroded and transported smectite from the same region that had previously been eroded through aeolian processes in the very-Early Cretaceous. This transition between illite-chlorite to smectite-kaolinite denotes a change in sedimentary provenance, however, it is difficult to precisely differentiate specific source-terranes without other provenance indicators such as heavy mineral analysis (Farrant et al., 2019), zircon geochronology (Fielding et al., 2018) and expanded isotopic studies (Mourlot et al., 2018b). A minor difference in the bulk-rock mineralogy is suggestive of a further, albeit subtle change in sedimentary provenance. The siliciclastic components for wells TB-1, NSO-1, Ti-1, Nd-1 and KaF-1 are mineralogically similar, containing varying proportions of quartz, feldspar, k-feldspar and phyllosilicates (chlorite, illite, kaolinite and smectite). However, the southernmost well CM-10 is devoid of K-feldspar and includes clinopyroxene (pigeonite) during the Lower Cretaceous which may infer a different sedimentary provenance, south or south-east of the onshore Senegalese Basin.

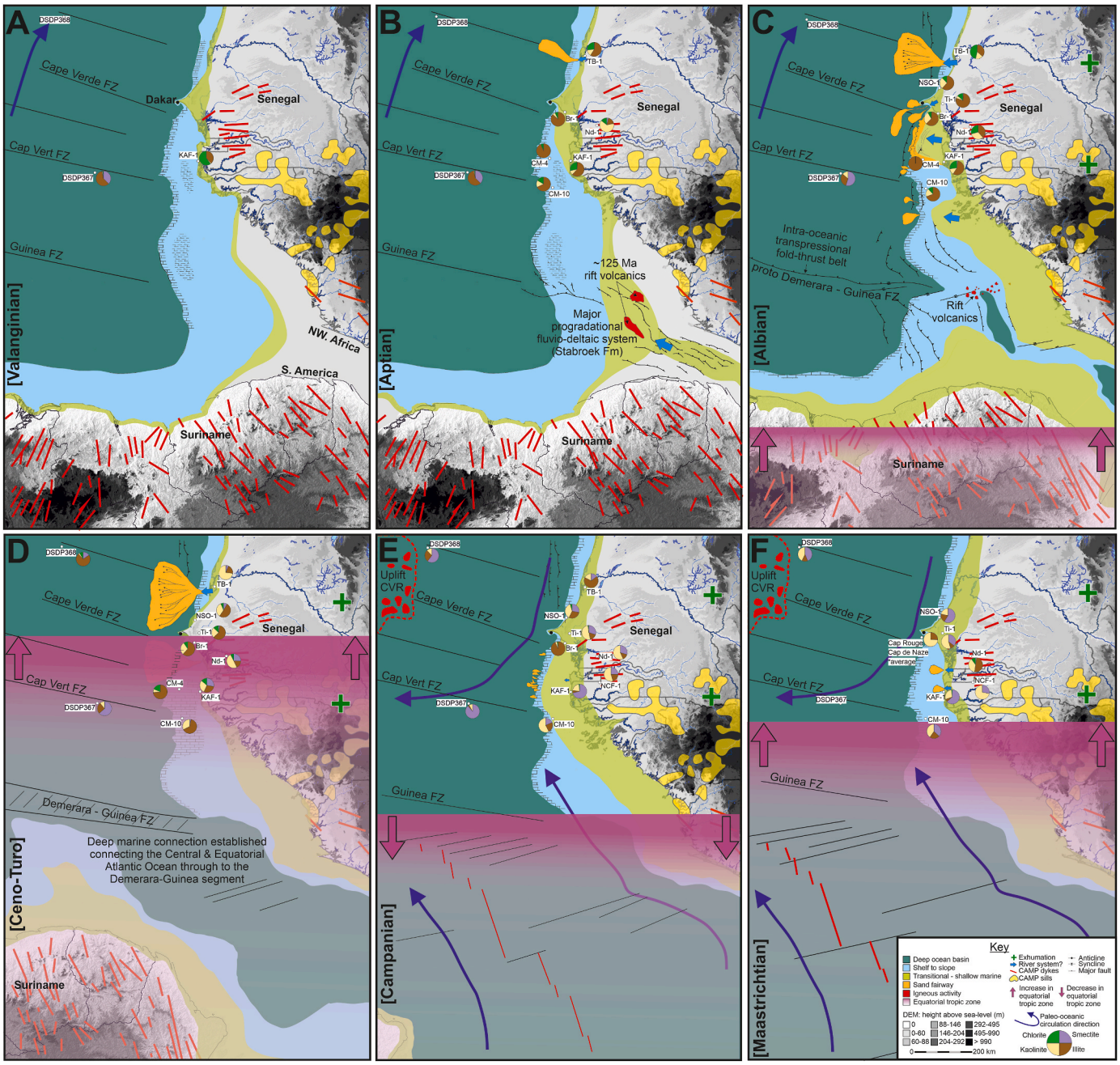

Fig. 11. Palaeogeographical reconstructions for six key Cretaceous intervals during the rifting of Atlantica: A, Valaginian (135 Ma); B, Aptian (125 Ma); C, Albian (113 Ma); D, Cenomanian-Turonian transition (94 Ma); E, Campanian (78 Ma); F, Maastrichtian (72 Ma). Tectonic geometries were reconstructed using Geognostics Earth Model (GEM™) with superimposed modern-day DEM and river networks from GEBCO (2021). For the purpose of this reconstruction Africa remains static in relation to the separation and rotation of South America. Sand fairways and shelf to slope replicated from Gross Depositional Environment (GDE) maps by Casson (2020c). Exhumation established from apatite fission track analysis by Gouiza et al. (2019) in the Mauritanides. Limits of the equatorial tropic zone from Hay and Floegal (2012). Palaeo-oceanic currents from Hay (2009). CAMP dyke and sill placement from Marzoli et al. (2018). CVR (Cape Verde rise).

5.3. Isotopic data

Provenance of CM-1 sediments was established by Mourlot et al. (2018[2]) and includes the Palaeozoic Taoudeni (εNd (0) −0.7) and Bove Basins, and Precambrian Mauritanides (εNd (0) −5.4), Kedougou-Kenieba-Inlier (KKI) and Leo-Man Shield (εNd (0) −17.9). Variable dilution between less-radiogenic Leo-Man Shield (−17.9) and the more-radiogenic Mauritanides (−5.4), and Taoudeni Basin (−0.7) source materials results in the range of εNd (0) values associated with CM-1 sediments (less radiogenic endmembers), TB-1 and Ti-1 sediments, ranging between −9 and −13 epsilon. Source 'α' sediments (Fig. 6 B) are slightly more radiogenic with an εNd (0) range of −9.17 to −10.79 epsilon, this group predominantly comprised of clay fractions associated with TB-1 suggesting a possible bias towards fluvially derived clays from the Mauritanides and/or the Taoudeni Basin. Source 'β' (Fig. 6 B) are comparatively less-radiogenic ranging between −11.26 and −12.78 potentially biased towards sediment derived from the Leo-Man Shield.

Strontium isotopes values recorded from TB-1 sediments display a greater disparity between the silt and clay fractions from the Aptian to Cenomanian, with a recognised depletion of radiogenic Sr within the clay fraction inferring increased humidity and potential for chemical weathering (Meyer et al., 2011). Comparable Campanian $^{87}Sr/^{86}Sr$

values infer a reduction in chemical weathering, but not a total cessation, as this would be indicated by a greater propensity to increased radiogenic Sr in the clay fraction. Ti-1 sediments display less isotopic Sr and Nd variation between the clay and silt fraction reaffirming a single and potentially more proximal source whereby there is less time for chemical weathering to occur between the erosion and deposition of the sediment into the central Senegal onshore Basin.

6. Conclusion

We utilise a wealth of extracted mineralogical data from published literature combined with new data collected for this study to analyses and interpret the causal mechanisms for climate change in NW Africa during the Cretaceous Period. The dominance of chlorite-illite clay from the Cretaceous shallow marine intervals from sampled wells offshore Senegal support an interpretation that Northwest Africa during the earliest Cretaceous (Berriasian-Aptian) was a barren arid environment with limited precipitation restricted to the farthest coastal regions, producing only modest fluvial systems draining relatively small catchments. This period of aridity, which extended back into the Jurassic period, would have provided optimal conditions for the development of authigenic smectite in the deeper hinterland. Monsoonal winds were the dominant mechanism for sediment delivery offshore, evidenced by smectite with subordinate illite recovered from samples in DSDP well sediments.

During the Albian, the continued fragmentation of Pangea, including opening of the juvenile EAG, and the associated evolution of the palaeo-ITCZ, contributed towards increased humidity within the tropics. This increase in humidity climaxed during the Cenomanian/Turonian marking the peak of the CTM. This is evidenced in well sample mineralogy by an increase in kaolinite content; a common proxy for increased chemical weathering of feldspathic source rocks. In particular, an increase in kaolinite during the Albian is observed in both DSDP wells 367 and 534 inferring a same periodicity for increased weathering rates on either side of the Central Atlantic Ocean. $^{87}Sr/^{86}Sr$ isotopes supports this model for increased weathering rates with pronounced depletion in radiogenic Sr from the clay fraction of TB-1 sediments; this infers a river-system analogous of the modern-day Senegal River which has a catchment which encompasses the western margin of the WAC extending into Mauritania, Mali and Guinea.

Throughout the CTM tropical humidity and precipitation increased considerably, generating larger river systems with greater catchments extending deeper into the hinterland, as evidenced by the shift to smectite and kaolinite plus illite within the nearshore sediments. Whilst atmospheric-continental humidity was elevated and denudation of the hinterland was accelerating, the eruption of the Caribbean LIP occurred causing the OAE2 in the North Atlantic Ocean. This provided the optimal conditions for palygorskite authigenesis of marine smectite, as observed in DSDP 367. Santonian and Campanian palygorskite within unit 2C of DSDP 368 may reflect ocean anoxia related to OAE3, although this is uncorroborated due to the indeterminate timing of localised ocean anoxia during the Late Cretaceous. However, given the proximity of DSDP 368 to the Cape Verde Rise and the incidental timing for the initiation of Cape Verde volcanism; a causal association may be applied linking volcanically-derived WSBW and the authigenesis of marine smectite.

Following the CTM NW Africa returned to a tropical climate, albeit hotter in comparison to modern-day standards. As the climate evolved throughout the Cretaceous so did the local vegetation, evolving into flora associated with hot and damp "swamp-like" environments acting to capture most of the channelised sediment within the onshore Senegalese Basin.

This study has demonstrated a clear antithetical change in climate during the Cretaceous, which is observed in the rock record. However, throughout this investigation two fundamental observations should be considered.

1. A literature review of atmospheric CO_2 concentration during the Cretaceous has revealed a growing consensus that levels actually declined throughout the period, suggesting an alternative cause for the CTM besides CO_2. A "perfect-storm" of events leading up to the CTM occurred, including: sea-level rise and increased oceanic to continental surface area, changes in global meteorology and increased vegetation occupying higher latitudes. All these contributing factors have associations to an evapotranspiration positive feedback loop, identifying water vapor as a prime candidate for the cause of the CTM.
2. Because of rising global temperatures and the resulting loss of polar ice, combined with increased sedimentation and ocean ridge volumes; Cretaceous eustatic sea-levels rose to 200m above current levels. However, given the proximity of the NW Africa conjugate margin to the opening of mid-Atlantic Ridge, crustal updoming and/or underplating caused sufficient increases in dynamic topography to inhibit any marine transgression. This period of dynamic tectonism coincided with the PAAP and is evidenced by extensive CAMP dykes and sills along either side of the conjugate margin. This period of increased dynamic topography correlates aptly with the timing of WAC and Leo-Man shield uplift.

Author declaration

The authors declare that they have no known competing financial interests or personal relationships that could have appeared to influence the work reported in this paper. [Instructions: Please check all applicable boxes and provide additional information as requested.]

Funding

No funding was received for this work.

Intellectual property

We confirm that we have given due consideration to the protection of intellectual property associated with this work and that there are no impediments to publication, including the timing of publication, with respect to intellectual property. In so doing we confirm that we have followed the regulations of our institutions concerning intellectual property.

Research ethics

We further confirm that any aspect of the work covered in this manuscript that has involved human patients has been conducted with the ethical approval of all relevant bodies and that such approvals are acknowledged within the manuscript.

Written consent to publish potentially identifying information, such as details or the case and photographs, was obtained from the patient(s) or their legal guardian(s).

Authorship

We confirm that the manuscript has been read and approved by all named authors.

We confirm that the order of authors listed in the manuscript has been approved by all named authors.

CRediT authorship contribution statement

M. Pearson: Writing – review & editing, Writing – original draft, Methodology, Investigation, Formal analysis, Data curation, Conceptualization. **M. Casson:** Writing – review & editing, Supervision, Investigation. **I. Millar:** Validation, Data curation. **R. Charton:** Writing –

review & editing. **J. Redfern:** Writing – review & editing, Supervision, Project administration, Funding acquisition.

Declaration of competing interest

Potential conflict of interest exists.

Data availability

Data will be made available on request.

Acknowledgements

This study is part of the lead authors PhD project at the University of Manchester. We thank the sponsoring companies of the North African Research Group (NARG) for their continued financial and scientific support. Special thanks to the DSDP core repository at the University of Bremen, Germany and to Petrosen in Dakar, Senegal for access to their core and cuttings repository. Finally, thanks to the British Geological Survey for their support and analytical facilities.

References

Adloff, M., Greene, S.E., Parkinson, I.J., Naafs, B.D.A., Preston, W., Ridgwell, A., Lunt, D. J., Jiménez, J.M.C., Monteiro, F.M., 2020. Unravelling the sources of carbon emissions at the onset of Oceanic Anoxic Event (OAE) 1a. Earth Planet Sci. Lett. 530 https://doi.org/10.1016/j.epsl.2019.115947.

Akinlotan, O.O., Moghalu, O.A., Hatter, S.J., Okunuwadje, S., Anquilano, L., Onwukwe, U., Haghani, S., Anyiam, O.A., Jolly, B.A., 2022. Clay mineral formation and transformation in non-marine environments and implications for Early Cretaceous palaeoclimatic evolution: the Weald Basin, Southeast England. J. Palaeogeogr. 11 (3), 387–409. https://doi.org/10.1016/j.jop.2022.04.002.

Anderson, T.R., Hawkins, E., Jones, P.D., 2016. CO2, the greenhouse effect and global warming: from the pioneering work of Arrhenius and Callendar to today's Earth System Models. Endeavour 40 (3), 178–187. https://doi.org/10.1016/j.endeavour.2016.07.002.

Arantegui, A., Jerrett, R., Schröder, S., Bulot, L.G., Gatto, R., Monari, S., Redfern, J., 2019. Constraining Mesozoic early post-rift depositional systems evolution along the eastern Central Atlantic margin. Sediment. Geol. 386, 31–51. https://doi.org/10.1016/j.sedgeo.2019.03.005.

Atlantic and Atlas regions by Antonio Schettino and Eugenio Turco. Geophys. J. Int., 183, 96-98. https://doi.org/10.1111/j.1365-246X.2010.04740.x..

Bakun, A., Field, D.B., Redondo-Rodriguez, A., Weeks, S.J., 2010. Greenhouse gas, upwelling-favourable winds, and the future of coastal ocean upwelling ecosystems. Global Change Biol. 16, 1213–1228. https://doi.org/10.1111/j.1365-2486.2009.02094.x.

Barusseau, J.P., Roger, J., Noel, B.J., Serrano, O., Duvail, C., 2009. Notice explicative de la carte géologique du Sénégal à 1/200 000, feuilles de Saint-Louis–Dagana, Podor–Saldé, Matam Semmé. Ministère des Mines, de l'Industrie et des PME, Direction des Mines et de la Géologie. Dakar.

Bice, K.L., Norris, R.D., 2002. Possible atmospheric CO2 extremes of the middle cretaceous (late albian–turonian). Paleoceanogr. Paleoclimatol. 17 (4), 22. https://doi.org/10.1029/2002PA000778, 1-22-17.

Bird, A., Millar, I., Rodenburg, T., Stevens, T., Rittner, M., Vermeesch, P., Lu, H., 2020. A constant Chinese Loess Plateau dust source since the late Miocene. Quat. Sci. Rev. 227 https://doi.org/10.1016/j.quascirev.2019.106042.

Biscaye, P., 1965. Mineralogy and sedimentation of recent deep-sea clay in the Atlantic Ocean and adjacent seas and oceans. GSA Bulletin 76 (7), 803–832. https://doi.org/10.1130/0016-7606(1965)76[803:MASORD]2.0. CO;2.

Blenkinsop, T.G., Moore, A., 2013. Tectonic geomorphology of passive margins and continental hinterlands. Treatise on Geomorphology 5, 71–92. https://doi.org/10.1016/B978-0-12-374739-6.00083-X.

Bottini, C., Dieni, I., Erba, E., Massari, F., Weissert, H., 2018. The Valanginian Weissert oceanic anoxic event recorded in central-Eastern Sardinia (Italy). Research in Paleontology and stratigraphy 124 (3), 617–637.

Bouchouicha, H., 2022. "El Hamma, Algeria". https://unsplash.com/photos/DVePpDiWwyc.Accessed21stJune2022.

Brass, G.W., Saltzman, E., Sloan, J.L., Southam, J.R., Hay, W.W., Holser, W.T., Peterson, W.H., 1982. Ocean circulation, plate tectonics and climate. Climate in Earth History, Studies in Geophysics. https://doi.org/10.17226/11798.

Bretschneider, L., Hathorne, E.C., Huang, H., Lübbers, J., Kochhann, K.G.D., Holbourn, A., 2021. Provenance and weathering of clays delivered to the Bay of Bengal during the middle Miocene: linkages to tectonics and monsoonal climate. Paleoceanogr. Paleoclimatol. 36 (2) https://doi.org/10.1029/2020PA003917.

Brosse, E., 1982. Contribution à la minéralogie et à la géochimie des sédiments pélagiques profonds. Comparaison des "Black-Shales" du Crétacé dans l'Atlantique central nord et des dépôts du Malm et du Crétacé en Briançonnais. Thèse Docteur-Ingénieur. Ecole Nationale Supérieure des Mines de Paris.

Buchs, D.M., Kerr, A.C., Brims, J.C., Zapata-Villada, J.P., Correa-Restrepo, T., Rodríguez, G., 2018. Evidence for subaerial development of the Caribbean oceanic plateau in the Late Cretaceous and paleo-environmental implications. Earth Planet Sci. Lett. 499, 62–73. https://doi.org/10.1016/j.epsl.2018.07.020.

Casson, M., Bulot, L., Jeremiah, J., Redfern, J., 2020a. Deep sea rock record exhumed on oceanic volcanic islands: the Cretaceous sediments of Maio, Cape Verde. Gondwana Res. 81, 252–264. https://doi.org/10.1016/j.gr.2019.11.007.

Casson, M., Calves, G., Huuse, M., Sayers, B., Redfern, J., 2020b. Cretaceous continental margin evolution revealed using quantitative seismic geomorphology, offshore northwest Africa. Basin Res. 33 (12) https://doi.org/10.1111/bre.12455.

Casson, M.A., 2020c. Tectono-stratigraphic Evolution of the Mesozoic Continental Margins of the Central Atlantic. A thesis submitted to the University of Manchester (Chapter 6).

Chamley, H., Debrabant, P., Candillier, A.-M., Foulon, J., 1983. Clay mineralogical and inorganic geochemical stratigraphy of blake-bahama basin since the callovian, site 534, deep sea drilling project leg 76. Geology, geography. Environ. Sci. J. Integr. Environ. Res. https://doi.org/10.2973/DSDP.PROC.76.113.1983.

Chamley, H., Debrabant, P., Flicoteaux, R., 1988. Comparative evolution of the Senegal and eastern central Atlantic Basins, from mineralogical and geochemical investigations. Sedimentology 35, 85–103. https://doi.org/10.1111/j.1365-3091.1988.tb00906.x.

Charton, R., 2018. Phanerozoic vertical movements in Morocco. Applied Geology, Thesis ISBNs978–94, 6186, 913-5.

Charton, R., Bertotti, G., Arantehui, A., Bulot, L.C., 2018. The Sidi Ifni transect across the rifted margin of Morocco (Central Atlantic): vertical movements constrained by low-temperature thermochronology. J. Afr. Earth Sci. 141, 22–32. https://doi.org/10.1016/j.jafrearsci.2018.01.006.

Charton, R., Bertotti, G., Arnould, A.D., Storms, J.E.A., Redfern, J., 2021. Low-temperature thermochronology as a control on vertical movements for semi-quantitative source-to-sink analysis: a case study for the Permian to Neogene of Morocco and surroundings. Basin Res. 33 (2), 1337–1383. https://doi.org/10.1111/bre.12517.

Chiarenza, A.A., Farnsworth, A., Mannion, P.D., Allison, P.A., 2020. Asteroid impact, not volcanism, caused the end-Cretaceous dinosaur extinction. Proc. Natl. Acad. Sci. USA 117 (29). https://doi.org/10.1073/pnas.2006087117.

Clayburn, J., 2018. Realising the Deep Water Hydrocarbon Potential of Senegal. Search and Discovery Article #70345. Adapted from Oral Presentation Given at the Discovery Thinking Forum AAPG/SEG 2017 International Conference and Exhibition. London, England.

Cox, K.G., 1993. Continental magmatic underplating. Phil. Trans. Phys. Sci. Eng. 342 (1663), 155–166. https://www.jstor.org/stable/54188.

Curioso Photography, 2020. In: "Senegal". https://unsplash.com/photos/OOiygaquXZs, 21st June 2022.

Danzelle, J., Riquier, L., Baudin, F., Thomazo, C., Pucéat, E., 2018. Oscillating redox conditions in the vocontian basin (SE France) during oceanic anoxic event 2 (OAE 2). Chem. Geol. 493, 136–152. https://doi.org/10.1016/j.chemgeo.2018.05.039.

David, W.J., 2017. The relationship between atmospheric carbon dioxide concentration and global temperature for the last 425 million years. Climate 5 (4), 76. https://doi.org/10.3390/cli5040076.

Dodsworth, R., Eldrett, J.S., Hard, M.B., 2020. Cretaceous oceanic anoxic event 2 in eastern england: further palynological and geochemical data from melton ross. Proc. Yorks. Geol. Soc. 63, 88–123. https://doi.org/10.1144/pygs2019-017.

Fairhead, J.D., 2023. The mesozoic west and central Africa Rift System (WCARS) and the older kandi shear zone (KSZ): rifting and tectonics of North Africa and SouthSouth America and fragmentation of Gondwana based on geophysical investigations. J. Afr. Earth Sci. 199 https://doi.org/10.1016/j.jafrearsci.2022.104817.

Farrant, A.R., Mounteney, I., Burton, A., Thomas, R.J., Roberts, N.M., Knox, R.W., Bide, T., 2019. Gone with the wind: dune provenance and sediment recycling in the northern Rub'al-Khali, United Arab Emirates. J. Geol. Soc. 176 (2), 269–283. https://doi.org/10.1144/jgs2017-044.

Fathy, D., Wagreich, M., Fathi, E., Ahmed, M.S., Leila, M., Sami, M., 2023. Maastrichtian anoxia and its influence on organic matter and trace metal patterns in the southern tethys realm of Egypt during greenhouse variability. ACS Omega 8 (22), 19603–19612. https://doi.org/10.1021/acsomega.3c01096.

Fielding, L., Najman, Y., Millar, Butterworth, P., Garzanti, E., Vezzoli, G., Barfod, D., Kneller, B., 2018. The initiation and evolution of the River Nile. Earth Planet Sci. Lett. 489, 166–178. https://doi.org/10.1016/j.epsl.2018.02.031.

GEBCO Compilation Group, 2021. GEBCO Grid. https://doi.org/10.5285/c6612cbe-50b3-0cff-e053-6c86abc09f8f.

GEM, 2020. Geognostics Earth Model. https://www.geognostics.com/.

Gertsch, B., Adatte, T., Keller, G., Aziz, A., Tantawy, A.M., Berner, Z., Mort, H.P., Fleitmann, D., 2010. Middle and late Cenomanian oceanic anoxic events in shallow and deeper shelf environments of western Morocco. Sedimentology 57, 1430–1462.

Gilchrist, A.R., Summerfield, M.A., 1994. Tectonic models of passive margin evolution and their implication for theories of long-term landscape development. Process Models and Theoretical Geomorphology 55–84.

Gouiza, M., Bertotti, G., Charton, R., Haimoudane, K., Dunkl, I., Anczkiewicz, A., 2019. New evidence of 'Anomalous' vertical movements along the hinterland of the atlantic NW african margin. J. Geophys. Res. Solid Earth 124 (12), 13333–13353. https://doi.org/10.1029/2019JB017914.

Graciansky, P.C., Brosse, E., Deroo, G., Herbin, J.P., Montardet, L., Müller, C., Sigal, J., Schaaf, A., 1987. Organic-rich sediments and paleoenvironmental reconstruction of the cretaceous North Atlantic. Marine Petroleum Source Rocks 26, 317–344. Geological Society Special Publication.

Grossenbacher, N., 2022. Untitled. https://unsplash.com/photos/WwCTwAE7rPA, 21st June 2022.

Haq, B.U., Huber, B.T., 2017. Anatomy of a eustatic event during the Turonian (Late Cretaceous) hot greenhouse climate. Sci. China Earth Sci. 60, 20–29. https://doi.org/10.1007/s11430-016-0166-y.
Hay, W.W., 2009. Cretaceous oceans and ocean modelling. Cretaceous Oceanic Red Beds: Stratigraphy, Composition, Origins, and Paleoceanographic and Paleoclimatic 243–271. Significance SEPM Special Publication, No. 91. ISBN 978-1-56576-135-3.
Hay, W.W., DeConto, R.M., de Boer, P., Flögel, S., Song, Y., Stepashko, A., 2019. Possible solutions to several enigmas of Cretaceous climate. Int. J. Earth Sci. 108, 587–620. https://doi.org/10.1007/s00531-018-1670-2.
Hay, W.W., Floegal, S., 2012. New thoughts about the Cretaceous climate and oceans. Earth Sci. Rev. 115 (4), 262–272. https://doi.org/10.1016/j.earscirev.2012.09.008.
Heimhofer, U., Wucherpfennig, N., Adatte, T., Schouten, S., Schneebeli-Hermann, E., Gardin, S., Keller, G., Kentsch, S., Kujau, A., 2018. Vegetation response to exceptional global warmth during Oceanic Anoxic Event 2. Nat. Commun. 9 (3832) https://doi.org/10.1038/s41467-018-06319-6.
Held, I.M., Soden, B.J., 2000. Water vapor feedback and global warming. Annu. Rev. Energy Environ. 25, 441–475. https://doi.org/10.1146/annurev.energy.25.1.441.
Holz, D.J., Williard, K.W.J., Edwards, P.J., Schoonover, J.E., 2015. Soil erosion in humid regions: a review. Journal of contemporary Water research & Education 154, 48–59. https://doi.org/10.1111/j.1936-704X.2015.03187.x.
Huber, B.T., MacLeod, K.G., Watkins, D.K., Coffin, M.F., 2018. The rise and fall of the Cretaceous Hot Greenhouse climate. Global Planet. Change 167, 1–23. https://doi.org/10.1016/j.gloplacha.2018.04.004.
Hülse, D., Arndt, S., Ridgwell, A., 2019. Mitigation of extreme ocean anoxic event conditions by organic matter sulfurization. Paleoceanogr. Paleoclimatol. 34, 476–789. https://doi.org/10.1029/2018PA003470.
Kemp, S.J., Ellis, M.A., Mounteney, I., Kender, S., 2016. Palaeoclimatic implications of high-resolution clay mineral assemblages preceding and across the onset of the palaeocene–eocene thermal maximum, north sea basin. Clay Miner. 51, 793–813. https://doi.org/10.1180/claymin.2016.051.5.08.
Kunzmann, L., Mohr, B., Bernardes-de-Oliveira, M., Wilde, V., 2006. Gymnosperms from the early cretaceous crato formation (Brazil). II. Cheirolepidiaceae. Fossil Record 9, 213–225. https://doi.org/10.1002/mmng.200600009.
Labails, C., Olivet, J.-L., Daniel, A., Roest, W.R., 2010. An alternative early opening scenario for the Central Atlantic Ocean. Earth Planet Sci. Lett. 297 (3), 355–368. https://doi.org/10.1016/j.epsl.2010.06.024.
Lamont-Doherty, Y.L., Bukry, D., 1978a. Site 367: Cape Verde Basin. https://doi.org/10.2973/dsdp.proc.41.103.
Lamont-Doherty, Y.L., Bukry, D., 1978b. Site 368: Cape Verde Basin. https://doi.org/10.2973/dsdp.proc.41.104.
Landing, E., 2012. Time-specific black mudstones and global hyper warming on the Cambrian–Ordovician slope and shelf of the Laurentia palaeocontinent. Palaeogeogr. Palaeoclimatol. Palaeoecol. 256–272. https://doi.org/10.1016/j.palaeo.2011.09.005.
Le Voyer, M., Hauri, E., Cottrell, E., Kelley, K., Salters, V., Langmuir, C., Hilton, D., Barry, P., Füri, E., 2018. Carbon fluxes and primary magma CO2 contents along the global mid-Ocean Ridge system. G-cubed 20 (3), 1387–1424. https://doi.org/10.1029/2018GC007630.
Leckie, M.R., Bralower, T.J., Cashman, R., 2002. Oceanic anoxic events and plankton evolution: biotic response to tectonic forcing during the mid-Cretaceous. Paleoceanography 17 (3).
Liu, W., Wu, H., Hinnov, L.A., Xi, D., He, H., Zhang, S., Yang, T., 2020. Early cretaceous terrestrial milankovitch cycles in the luanping basin, north China and time constraints on early stage jehol biota evolution. Front. Earth Sci. 8 (178) https://doi.org/10.3389/feart.2020.00178.
Lobkovsky, L.I., Shipilov, E.V., Kononov, M.V., 2013. Geodynamic model of upper mantle convection and transformations of the arctic lithosphere in the mesozoic and cenozoic. Phys. Solid Earth 49 (6), 767–785. https://doi.org/10.1134/S1069351313060104.
Lowery, C.M., Mark Leckie, R., Bryant, R., Elderbak, K., Parker, A., Polyak, D.E., Schmidt, M., Snoeyenbos-West, O., Sterzinar, E., 2018. The Late Cretaceous Western Interior Seaway as a model for oxygenation change in epicontinental restricted basins. Earth Sci. Rev. 177, 545–564. https://doi.org/10.1016/j.earscirev.2017.12.001.
Luber, T.L., Bulot, L.G., Redfern, J., Nahim, M., Jeremiah, J., Simmons, M., Bodin, M., Masrour, M., 2018. A revised chronostratigraphic framework for the Aptian of the Essaouira-Agadir Basin, a candidate type section for the NW African Atlantic Margin. Cretac. Res. 93, 292–317. https://doi.org/10.1016/j.cretres.2018.09.007.
Martin, J.E., Amiot, R., Lécuyer, C., Benton, M.J., 2014. Sea surface temperature contributes to marine crocodylomorph evolution. Nat. Commun. 5 (4658) https://doi.org/10.1038/ncomms5658.
Martin, L., Effimoff, I., Medou, J., Laughland, M., 2010. Hydrocarbon Prospectivity of Offshore Senegal - Unlocking the Door to a New Deepwater Petroleum. Search and Discovery Article #10278. Adapted from Oral Presentation at AAPG Convention. Louisiana, New Orleans.
Marzoli, A., Callegaro, S., Dal Corso, J., Davies, J.H.F.L., Chiaradia, M., Youbi, N., Bertrand, H., Reisberg, L., Merle, R., Jourdan, F., 2018. The central atlantic magmatic province (CAMP): a review. The Late Triassic World 46, 91–125. https://doi.org/10.1007/978-3-319-68009-5_4.
Marzoli, A., Renne, P., Piccirillo, E., Ernesto, M., Bellieni, G., De Min, Angelo, 1999. Extensive 200-million-year-old continental flood basalts of the central atlantic magmatic province. Science 284 (5414), 616–618. https://doi.org/10.1126/science.284.5414.616.
Matton, G., Jébrak, M., 2009. The Cretaceous Peri-Atlantic Alkaline Pulse (PAAP): deep mantle plume origin or shallow lithospheric break-up? Tectonophysics 469, 1–12. https://doi.org/10.1016/j.tecto.2009.01.001.
Meyer, I., Davies, G.R., Stuut, J.-B., 2011. Grain size control on Sr-Nd isotope provenance studies and impact on paleoclimate reconstructions: an example from deep-sea sediments offshore NW Africa. G-cubed 12 (3). https://doi.org/10.1029/2010GC003355.
Monteiro, F.M., Pancost, R.D., Ridgwell, A., Donnadieu, Y., 2012. Nutrients as the dominant control on the spread of anoxia and euxinia across the Cenomanian-Turonian oceanic anoxic event (OAE2): model-data comparison. Paleoceanography 27. https://doi.org/10.1029/2012PA002351.
Moreno, A., Targarona, J., Henderiks, J., Canals, M., Freudenthal, T., Meggers, H., 2001. Orbital forcing of dust supply to the North Canary Basin over the last 250 kyr. Quat. Sci. Rev. 20 (12), 1327–1339. https://doi.org/10.1016/S0277-3791(00)00184-0.
Morsi, A.-M., Faris, M., Zalat, A., Salem, R., 2008. Maastrichtian-Early Eocene ostracods from west-central Sinai, Egypt - taxonomy, biostratigraphy, paleoecology and paleobiogeography. Rev. Paleobiol. 27.
Mounteney, I., Casson, M., Rushton, J., Millar, I., Dethie, N., Redfern, J., 2021. Cenozoic to modern-day source to sink systems of Senegal: a record of provenance, transport, recycling and climate controls. African Earth Sciences 178, 104150. https://doi.org/10.1016/j.jafrearsci.2021.104150.
Mourlot, Y., Calves, G., Clift, P.D., Baby, G., Chaboureau, A.C., Raisson, F., 2018a. Seismic stratigraphy of cretaceous eastern central Atlantic Ocean: basin evolution and palaeoceanographic implications. Earth Planet Sci. Lett. 499 (10) https://doi.org/10.1016/j.epsl.2018.07.023.
Mourlot, Y., Roddaz, M., Dera, G., Calves, G., Kim, J.-H., Chaboureau, A.-C., Mounic, S., Raisson, F., 2018b. Geochemical evidence for large-scale drainage reorganization in Northwest Africa during the cretaceous. G-cubed 19, 1690–1712. https://doi.org/10.1029/2018GC007448.
Müller, D.R., Dutkiewicz, A., 2018. Oceanic crustal carbon cycle drives 26-million-year atmospheric carbon dioxide periodicities. Sci. Adv. 4 (2) https://doi.org/10.1126/sciadv.aaq0500.
Ndiaye, M., Ngom, P.M., Gorin, G., Villeneuve, M., Sartori, M., Medou, J., 2016. A new interpretation of the deep-part of Senegal-Mauritanian Basin in the Diourbel-Thies area by integrating seismic, magnetic, gravimetric and borehole data: implication for petroleum exploration. African Earth Sciences 121, 330–341. https://doi.org/10.1016/j.jafrearsci.2016.06.002.
Nicholson, U., Bray, V.J., Gulick, S.P.S., Aduomahor, B., 2022. The Nadir crater offshore West Africa: a candidate cretaceous-paleogene impact structure. Sci. Adv. 8, 33. https://doi.org/10.1126/sciadv.abn3096.
Park, J., D'Hondt, S.L., King, J.W., Gibson, C., 1993. Late cretaceous precessional cycles in double time: a warm-earth milankovitch response. Science 261, 1431–1434. https://doi.org/10.1126/science.261.5127.1431.
Pérez-Díaz, L., Eagles, G., 2017. South atlantic paleobathymetry since early cretaceous. Sci. Rep. 7 (11819) https://doi.org/10.1038/s41598-017-11959-7.
Pierrehumbert, R.T., 2002. The hydrologic cycle in deep-time climate problems. Nature 419, 191–198. https://doi.org/10.1038/nature01088.
Pletsch, T., Erbacher, J., Holburn, A.E.L., Kuhnt, W., Moullade, M., Oboh-Ikuenobede, F. E., Söding, E., Wagner, T., 2001. Cretaceous separation of Africa and SouthSouth America: the view from the West african margin (ODP leg 159). J. S. Am. Earth Sci. 14, 147–174. https://doi.org/10.1016/S0895-9811(01)00020-7.
Pogge von Strandmann, P.A.E., Jenkyns, H.C., Woodfine, R.G., 2013. Lithium isotope evidence for enhanced hydrological cycling during Oceanic Anoxic Event 2. Nat. Geosci. 6 (8), 668–672. https://doi.org/10.1038/ngeo1875.
Poulsen, C.J., Gendaszek, A.S., Jacob, R.L., 2013. Did the rifting of the Atlantic Ocean cause the Cretaceous thermal maximum? Geology 31 (2). https://doi.org/10.1130/0091-7613(2003)031<0115:DTROTA>2.0. CO;2.
Pu, K., Cook, K.H., 2010. Dynamics of the West African westerly jet. J. Clim. 23 (23), 6263–6276. https://doi.org/10.1175/2010JCLI3648.1.
Robock, A., Outten, S., Volcanoes: Role in Climate, doi: 10.1016/B978-0-12-409548-9.11423-X.
Rogers, J.J.W., 1996. A history of the continents in the past three billion years. J. Geol. 104 (1) https://doi.org/10.1086/629803.
Rogers, J.J.W., Santosh, M., 2003. Supercontinents in Earth history. Gondwana Res. 6 (3), 357–368. https://doi.org/10.1016/S1342-937X(05)70993-X.
Rothman, D.H., 2002. Atmospheric carbon dioxide levels for the last 500 million years. Proc. Natl. Acad. Sci. USA 99 (7), 4167–4171. https://doi.org/10.1073/pnas.022055499.
Salard-Cheboldaeff, M., Dejax, J., 1991. Evidence of Cretaceous to Recent West African intertropical vegetation from continental sediment spore-pollen analysis. J. Afr. Earth Sci. 12, 353–361. https://doi.org/10.1016/0899-5362(91)90084-C.
Scherer, C.M.S., Mello, R.G., Ferronatto, J.P.F., Amarante, F.B., Reis, A.D., Souza, E.G., Goldberg, K., 2020. Changes in prevailing surface-palaeowinds of western Gondwana during early cretaceous. Cretac. Res. 116 https://doi.org/10.1016/j.cretres.2020.104598.
Schimmeck, A., 2021. "Valley of the Ziz, Morocco". https://unsplash.com/photos/uzM1XBFqa60, 21st June 2022.
Scotese, C., 2004. Cenozoic and mesozoic paleogeography: changing terrestrial biogeographic pathways. Frontiers of Biogeography: New Directions in the Geography of Nature (Chapter 1).
Scotese, C.R., 2021. Phanerozoic paleotemperatures: the Earth's changing climate during the last 540 million years. Earth Sci. Rev. https://doi.org/10.1016/j.earscirev.2021.103503.
Sellwood, B.W., Valdes, P.J., 2006. Mesozoic climates: general circulation models and the rock record. Sediment. Geol. 190, 269–287. https://doi.org/10.1016/j.sedgeo.2006.05.013.
Sewall, J.O., van de Wal, R.S.W., van der Zwan, K., van Oosterhout, C., Diijkstra, H.A., Scotese, C.R., 2007. Climate model boundary conditions for four Cretaceous time slices. Clim. Past 3, 647–657. https://doi.org/10.5194/cp-3-647-2007.

Sheridan, R.E., Gradstein, F.M., 1980. Blake-Bahama Basin. https://doi.org/10.2973/dsdp.proc.76.104.

Stuut, J.-B., Zabel, M., Ratmeyer, V., Helmke, P., Schefuß, E., 2005. Provenance of present-day aeolian dust collected off NW Africa. J. Geophys. Res. 110 https://doi.org/10.1029/2004JD005161.

Svensen, H.H., Callegaro, S., Augland, L., Hatlen Heimdal, T., Jerram, D., Planke, S., Pereira, E., 2017. Gondwana Large Igneous Provinces: Plate Reconstructions, Volcanic Basins and Sill Volumes. Geological Society, London. https://doi.org/10.1144/SP463.7. Special Publications. 463.

Takashima, R., Nishi, H., Huber, B.T., Leckie, M., 2006. Greenhouse world and the mesozoic ocean. Oceanography 19 (4), 64–74. https://doi.org/10.5670/oceanog.2006.07.

Taylor, B., 2006. The single largest oceanic plateau: Ontong Java–Manihiki–Hikurangi. Earth Planet Sci. Lett. 241, 372–380. https://doi.org/10.1016/j.epsl.2005.11.049.

Taylor, S.R., McLennan, S.M., 1985. The Continental Crust: its Composition and Evolution. Blackwell Scientific Publications, p. 312p.

Thiry, M., Pletsch, T., 2011. Palygorskite clays in marine sediments: records of extreme climate. Developments in Clay Science 3, 101–124. https://doi.org/10.1016/B978-0-444-53607-5.00005-0.

Torsvik, T.H., Dietmar Muller, R., Van der Voo, R., Steinberger, B., Gaina, C., 2008. Global plate motion frames: toward a unified model. Rev. Geophys. 46 (3) https://doi.org/10.1029/2007RG000227.

Tuite Jr., M.L., Williford, K.H., Macko, S.A., 2019. From greenhouse to icehouse: nitrogen biogeochemistry of an epeiric sea in the context of the oxygenation of the Late Devonian atmosphere/ocean system. Palaeogeogr. Palaeoclimatol. Palaeoecol. 531, 109204 https://doi.org/10.1016/j.palaeo.2019.05.026.

Turgeon, S.C., Creaser, R.A., 2008. Cretaceous oceanic anoxic event 2 triggered by a massive magmatic episode. Nature 454, 232–326. https://doi.org/10.1038/nature07076.

Wagreich, M., 2012. "OAE 3" – regional Atlantic organic carbon burial during the Coniacian–Santonian. Clim. Past 8, 1447–1455. https://doi.org/10.5194/cp-8-1447-2012.

Wang, H., Dilcher, D.L., 2006. Aquatic angiosperms from the Dakota formation (albian, lower cretaceous), hoisington III locality, Kansas, USA. Int. J. Plant Sci. 167 (2), 385–401. https://doi.org/10.1086/499502.

Watson, J., 1985. Northern Scotland as an atlantic-north sea divide. J. Geol. Soc. 142, 221–243. https://doi.org/10.1144/gsjgs.142.2.0221.

Whalen, M.T., Gulick, S.P.S., Lowery, C.M., Bralower, T.J., Morgan, J.V., Grice, K., Schaefer, B., Smit, J., Ormö, J., Wittmann, A., Kring, D.A., Lyons, S., Goderis, S., 2020. Winding down the Chicxulub impact: the transition between impact and normal marine sedimentation near ground zero. Mar. Geol. 430 https://doi.org/10.1016/j.margeo.2020.106368.

White, R.S., Mckenzie, D.P., 1989. Magmatism at rift zones: the generation of volcanic continental margins and flood basalts. J. Geophys. Res. 94, 7685–7730. https://doi.org/10.1029/JB094iB06p07685.

Wilson, P.A., Norris, R.D., Cooper, M.J., 2002. Testing the Cretaceous greenhouse hypothesis using glassy foraminiferal calcite from the core of the Turonian tropics on Demerara Rise. Geology 30 (7), 607–610. https://doi.org/10.1130/0091-7613(2002)030<0607:TTCGHU>2.0.CO, 2.

Winguth, A.M.E., Shields, C.A., Winguth, C., 2015. Transition into a hothouse World at the Permian–Triassic boundary—a model study. Palaeogeogr. Palaeoclimatol. Palaeoecol. 440, 316–327. https://doi.org/10.1016/j.palaeo.2015.09.008.

Wright, N.M., Seton, M., Williams, S.E., Whittaker, J.M., Dietmar Müller, R., 2020. Sea-level Fluctuations Driven by Changes in Global Ocean Basin Volume Following Supercontinent Break-Up. Earth-Science Reviews 208, 103293. https://doi.org/10.1016/j.earscirev.2020.103293.